2014-06

Increasing the endurance and payload capacity of unmanned aerial vehicles with thin-film photovoltaics

Carey, Seamus B.

Monterey, California: Naval Postgraduate School

NAVAL POSTGRADUATE SCHOOL

MONTEREY, CALIFORNIA

THESIS

INCREASING THE ENDURANCE AND PAYLOAD CAPACITY OF UNMANNED AERIAL VEHICLES WITH THIN-FILM PHOTOVOLTAICS

by

Seamus B. Carey

June 2014

Thesis Advisor:	Sherif Michael
Second Reader:	Alejandro Hernandez

Approved for public release; distribution is unlimited

THIS PAGE INTENTIONALLY LEFT BLANK

REPORT DOCUMENTATION PAGE			*Form Approved OMB No. 0704-0188*
Public reporting burden for this collection of information is estimated to average 1 hour per response, including the time for reviewing instruction, searching existing data sources, gathering and maintaining the data needed, and completing and reviewing the collection of information. Send comments regarding this burden estimate or any other aspect of this collection of information, including suggestions for reducing this burden, to Washington headquarters Services, Directorate for Information Operations and Reports, 1215 Jefferson Davis Highway, Suite 1204, Arlington, VA 22202-4302, and to the Office of Management and Budget, Paperwork Reduction Project (0704-0188) Washington DC 20503.			
1. AGENCY USE ONLY ***(Leave blank)***	**2. REPORT DATE** June 2014	**3. REPORT TYPE AND DATES COVERED** Master's Thesis	
4. TITLE AND SUBTITLE INCREASING THE ENDURANCE AND PAYLOAD CAPACITY OF UNMANNED AERIAL VEHICLES WITH THIN-FILM PHOTOVOLTAICS		**5. FUNDING NUMBERS**	
6. AUTHOR(S) Seamus B. Carey			
7. PERFORMING ORGANIZATION NAME(S) AND ADDRESS(ES) Naval Postgraduate School Monterey, CA 93943-5000		**8. PERFORMING ORGANIZATION REPORT NUMBER**	
9. SPONSORING /MONITORING AGENCY NAME(S) AND ADDRESS(ES) N/A		**10. SPONSORING/MONITORING AGENCY REPORT NUMBER**	
11. SUPPLEMENTARY NOTES The views expressed in this thesis are those of the author and do not reflect the official policy or position of the Department of Defense or the U.S. Government. IRB Protocol number ____N/A____.			
12a. DISTRIBUTION / AVAILABILITY STATEMENT Approved for public release; distribution is unlimited		**12b. DISTRIBUTION CODE**	

13. ABSTRACT (maximum 200 words)

Prior research has shown that the endurance of small unmanned aerial vehicles (UAV) can be significantly extended using thin film photovoltaic cells. The different power requirements of the RQ-11B Raven variants are explored in this thesis, and it is demonstrated that a CuInGaS2 (CIGS) solar array adhered to the wing of an RQ-11B not only extends the flight time but also expands the payload capacity of the platform.

Power requirements and existing endurance of the digital variant of the RQ-11B were measured to establish a baseline of the platform's performance and validate previous research. A modular wing with an integrated CIGS array was then designed and constructed to be incorporated with the existing power circuitry of the platform. The baseline tests were repeated to determine the power generated by the array and supplied to the digital RQ-11B. It was shown that a solar integrated RQ-11B has a larger payload capacity and extended endurance, while still maintaining the modular and expeditionary nature of the existing platform. The concept of this research may be applied to all unmanned aerial platforms in order to expand their power generation to operate simultaneous or demanding payloads without stressing the existing power supply.

14. SUBJECT TERMS Raven, RQ-11B, UAV, Solar Power, CIGS, Thin Film Photovoltaic			**15. NUMBER OF PAGES** 87
			16. PRICE CODE
17. SECURITY CLASSIFICATION OF REPORT Unclassified	**18. SECURITY CLASSIFICATION OF THIS PAGE** Unclassified	**19. SECURITY CLASSIFICATION OF ABSTRACT** Unclassified	**20. LIMITATION OF ABSTRACT** UU

NSN 7540-01-280-5500 Standard Form 298 (Rev. 2-89)
Prescribed by ANSI Std. 239-18

THIS PAGE INTENTIONALLY LEFT BLANK

Approved for public release; distribution is unlimited

INCREASING THE ENDURANCE AND PAYLOAD CAPACITY OF UNMANNED AERIAL VEHICLES WITH THIN-FILM PHOTOVOLTAICS

Seamus B. Carey
Captain, United States Marine Corps
B.S., United States Naval Academy, 2008

Submitted in partial fulfillment of the
requirements for the degree of

MASTER OF SCIENCE IN ELECTRICAL ENGINEERING

from the

NAVAL POSTGRADUATE SCHOOL
June 2014

Author: Seamus B. Carey

Approved by: Dr. Sherif Michael
Thesis Advisor

Dr. Alejandro S. Hernandez
Second Reader

Dr. Clark Robertson
Chair, Department of Electrical Engineering
Graduate School of Engineering and Applied Science

THIS PAGE INTENTIONALLY LEFT BLANK

ABSTRACT

Prior research has shown that the endurance of small unmanned aerial vehicles (UAV) can be significantly extended using thin film photovoltaic cells. The different power requirements of the RQ-11B Raven variants are explored in this thesis, and it is demonstrated that a CuInGaS2 (CIGS) solar array adhered to the wing of an RQ-11B not only extends the flight time but also expands the payload capacity of the platform.

Power requirements and existing endurance of the digital variant of the RQ-11B were measured to establish a baseline of the platform's performance and validate previous research. A modular wing with an integrated CIGS array was then designed and constructed to be incorporated with the existing power circuitry of the platform. The baseline tests were repeated to determine the power generated by the array and supplied to the digital RQ-11B. It was shown that a solar integrated RQ-11B has a larger payload capacity and extended endurance, while still maintaining the modular and expeditionary nature of the existing platform. The concept of this research may be applied to all unmanned aerial platforms in order to expand their power generation to operate simultaneous or demanding payloads without stressing the existing power supply.

THIS PAGE INTENTIONALLY LEFT BLANK

TABLE OF CONTENTS

LIST OF FIGURES

LIST OF TABLES

THIS PAGE INTENTIONALLY LEFT BLANK

LIST OF ACRONYMS AND ABBREVIATIONS

DOD	Department of Defense
UAV	unmanned aerial vehicle
ISR	intelligence surveillance and reconnaissance
PV	photovoltaic
TFPV	thin-film photovoltaic
CIGS	Cadmium Indium Gallium di-Selenide
AV	air vehicle
GCS	ground control station
IR	infrared
EO	Electro-Optical
DDL	Digital Data Link
NREL	National Renewable Energy Laboratory
CdS	Cadmium Sulfide
CdTe	Cadmium Telluride
c-Si	crystalline Silicon
MPPT	maximum power point tracker
STC	standard test conditions
Li-ion	Lithium ion

THIS PAGE INTENTIONALLY LEFT BLANK

EXECUTIVE SUMMARY

The recent budgetary restrictions for the Department of Defense (DOD) underscore the relative cost effectiveness of unmanned aerial vehicles (UAV), while the military push toward alternative sources of energy demands that those systems are efficient. As a result, extending the endurance and increasing the payload capacity of the existing UAV inventory becomes a priority to enhance the combat effectiveness of the warfighter and reduce operational costs for the DOD. Currently, military UAVs are limited by the size of their payload and endurance. The present endurance for a UAV depends on the characteristics of the individual platform; however, the small, electric platforms such as the RQ-11B Raven are employed by small units and are limited to an operating time of 60 to 90 minutes [1]. While this platform is an asset to the warfighter, its capabilities are restricted by the dismal endurance and limited payload. Longer persistence and a larger payload would reduce the small unit's reliance on a limited number of surveillance assets. Fortunately, being driven by a brushless direct-current (DC) electric motor, the RQ-11B platform is a prime candidate for renewable sources of energy. As such, the incorporation of photovoltaic (PV) technology would extend the battery life of the Raven system and greatly increase its operating endurance and payload capacity.

Previous research has demonstrated that it is a proven and viable endeavor to increase the endurance of small Group 1 UAVs through the application of thin film photovoltaic (TFPV) cells [2], [3]. The objective of this thesis is to investigate whether high efficiency $CuInGaSe_2$ (CIGS) cells, when applied to an RQ-11B Raven, will power the aircraft from dawn to dusk and simultaneously increase the payload capacity. To accomplish this objective, the multiple variants of the Raven UAV were explored, and the power requirements of the current payloads were determined. With this baseline, a modular array of CIGS was designed for the RQ-11B that maintains the modular and expeditionary characteristics of the existing system. The modular array required additional power circuitry to be integrated with the Raven. A maximum power point tracker (MPPT), in series with the array, controls the output by adjusting its relative impedance to match the load and provide the maximum power to the lithium ion battery

of the Raven UAV. Before the battery can receive the input power from the array, it is boosted to the necessary voltage by a DC-DC converter. In this research, the MPPT and boost controller were incorporated on the same circuit board. Finally, a battery balancer ensures that the individual cells of the lithium ion battery are charged equally and safely.

Prior to constructing the array and power circuitry, a baseline for the system was established. It was determined that the current, digital version of the RQ-11B Digital Data Link (DDL) required much more current for operation than previous variants of the UAV. In Figure 1, the current draw of the RQ-11B, DDL is compared to previous research with the analog variant of the Raven. The increase in current depicted in Figure 1 is indicative of a higher power requirement for the digital variant of the UAV. This result voided the predictions and calculations of previous research for the potential of TFPVs to completely power a Raven system with solar energy. As a result, further testing was required to determine the actual endurance of the digital platform and the increase in endurance made possible by a CIGS array.

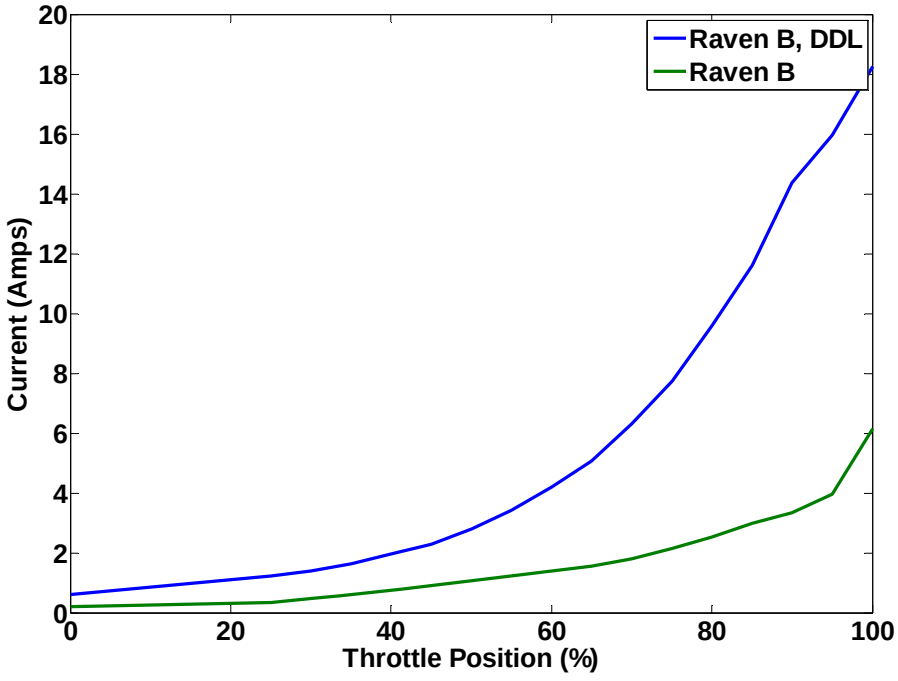

Figure 1. Average current draw of the Raven B, DDL variant at multiple throttle settings compared to the Raven B data (from [2]).

It was determined through multiple iterations of ground tests that the average endurance of the RQ-11B, DDL was approximately 30 minutes. This measurement was the time the UAV battery lasted before reaching a low voltage warning, indicating approximately 15 minutes of battery life remaining. By comparison, research in [3] with the analog version of the Raven measured an average baseline endurance of 126 minutes. This difference was consistent with the higher power requirements indicated by the current draw tests.

Once the endurance of the RQ-11B, DDL was established, the payloads were examined to determine their operating requirements. Through investigative analysis and multiple measurements, it was deduced that the various payloads of the Raven are powered by a maximum of 16.0 V and 187.0 mA. Assuming that the measured values were conservative with respect to the allowable energy requirements, we assumed that 6.0 W would be necessary for an array to power a single payload.

With a baseline for endurance and payload capacity established, the CIGS array was constructed and evaluated to determine its performance. With a surface area of 1828 cm^2 covered by CIGS, the array produced anywhere from 10.0 to 16.0 W depending on the solar irradiance and angle-of-incident light. With the MPPT integrated with the power circuitry, the array's output was held relatively constant at 14.0 W during optimal conditions. Once constructed and incorporated with the Raven, the array was evaluated with the same test procedures as baseline testing to determine the benefits provided by the CIGS. On average, the solar array enabled the AV to operate for nearly 45 minutes before receiving the low battery voltage warning. This endurance corresponds to a 48.87% improvement, which is shown in Figure 2. It was concluded that the improvements made to the Raven B, DDL variant drastically diminished the endurance benefits of incorporating a TFPV array with the power circuitry when compared to research in [3] and [4].

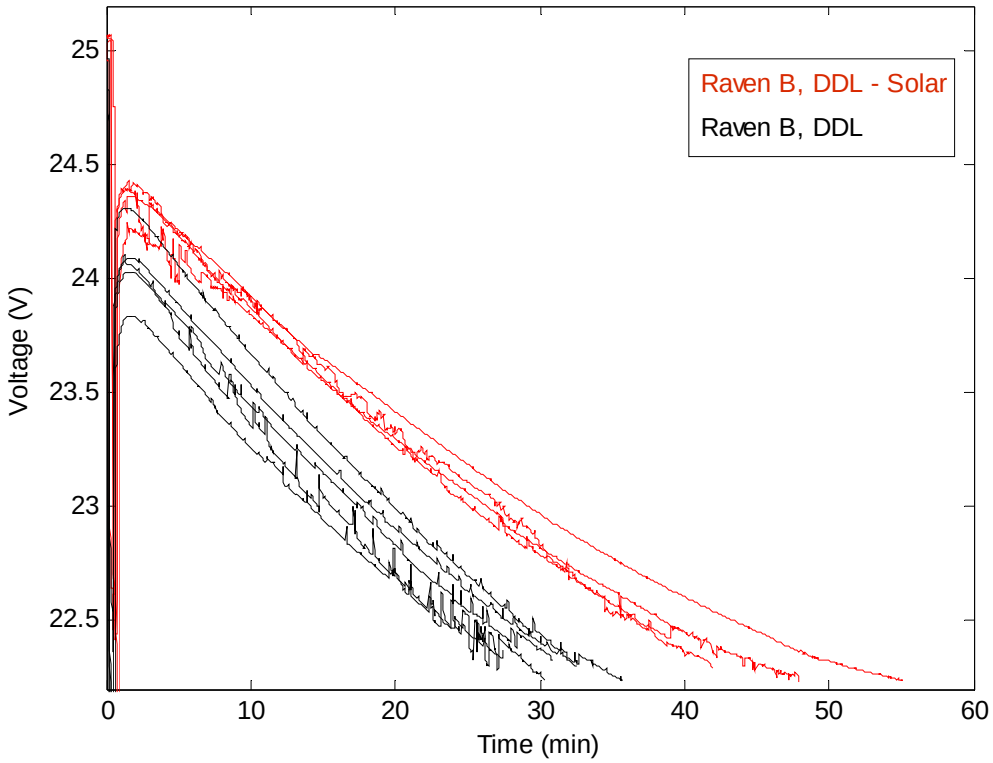

Figure 2. The results of a solar integrated Raven B, DDL endurance test compared to the baseline endurance.

While the endurance benefits were hampered by the improvements to the digital Raven platform, the power produced by the array may still be harnessed and applied elsewhere in the system. As previously mentioned, payload testing concluded that approximately 6.0 W are required to operate a single payload. The 14.0 W generated by low efficiency CIGS are more than sufficient to expand the payload capacity of the Raven.

Ultimately, with the current efficiencies of TFPVs and the increased power requirements of the Raven RQ-11B, DDL variant in mind, the concept of a solar powered Raven will not achieve realization. However, the benefits of a TFPV array integrated with the wing are not limited to endurance. An expansion of the payload capacity would benefit the warfighter by expanding the capabilities and the potential mission set of the

platform. Additionally, the solar wing would provide a much needed power source in austere and isolated environments.

The following recommendations for additional research are necessary to enhance and improve upon the findings of this research:

- Verify the current consumption of the Raven RQ-11B, DDL across the DOD inventory.
- Measure the current of the air vehicle in Autonomous Flight with a data logger.
- Conduct similar research with gas powered UAVs.
- Refine the wing interface design for the modular array.

LIST OF REFERENCES

[1] AeroVironment. (2014). *UAS: RQ-11B Raven* [Online]. Available: http://www.avinc.com/uas/small_uas/raven/.

[2] C. Gromadski, "Extending the endurance of small unmanned aerial vehicles using advanced flexible solar cells," M.S. thesis, Dept. of ECE, Naval Postgraduate School, Monterey, CA, 2012.

[3] J. V. Coba, "Application of Copper Indium Gallium Diselenide Photovoltaic Cells to Extend The Endurance and Capabilities of The Raven RQ-11B Unmanned Aerial Vehicle," M.S. thesis, Dept. of ECE, Naval Postgraduate School, Monterey, California, 2009.

[4] W. Hurd, "Application of cupper indium gallium diselenide photovoltaic cells to extend the endurance and capabilities of unmanned aerial vehicles," M.S. thesis, Dept. of ECE, Naval Postgraduate School, Monterey, CA, 2009.

THIS PAGE INTENTIONALLY LEFT BLANK

ACKNOWLEDGMENTS

I would like to extend my appreciation to all those who assisted me throughout the thesis process. If not for the help of gracious educators and Marines, I would have been unable to conduct this research. In particular, Sherif Michael, Jeff Knight, and James Calusdian were invaluable resources who sacrificed an inordinate amount of time explaining simple concepts to my simple mind. Additionally, I would like to thank the Marines at PMA-263, Naval Air Systems Command for providing me with the Raven system and giving me full reign to conduct the necessary investigation. Their support and responsiveness during this process has been superb.

Lastly, none of this would have been possible without the unrelenting love and support from my wife, Alexandra. She encourages, inspires, and surprises me every day.

THIS PAGE INTENTIONALLY LEFT BLANK

I. INTRODUCTION

A. BACKGROUND

Since 2001, the Department of Defense (DOD) utilization and acquisition of military unmanned aerial vehicles (UAV) has expanded exponentially [1]. The wars in Iraq and Afghanistan proved the usefulness and effectiveness of such systems in combat scenarios and provide a glimpse into the military and homeland security operations of the future. Despite the fiscal restrictions of the past few years, UAV production has resiliently increased, and the military spending on the acquisition of those systems is set to rise through fiscal year 2015 [1]. The tightening of the fiscal belt in Congress underscores the relative cost effectiveness of unmanned systems, while the military push toward alternative sources of energy demands that those systems are efficient. In particular, the commandant of the Marine Corps directs that the "the current and future operating environment requires an expeditionary mindset geared toward increased efficiency and reduced consumption, which will make our forces lighter and faster" [2]. As a result, extending the endurance and increasing the payload of tactical level UAVs becomes a priority to enhance the combat effectiveness of the warfighter and reduce operational costs for the DOD.

The asymmetrical style of warfare that experienced resurgence by the Global War on Terrorism has driven the desire to expand the UAV fleet. Currently, UAVs are organized into five different categories, Group 1 through Group 5. They are categorized according to the size, operating altitude, and airspeed of the individual platform. In Table 1, the five groups of UAVs are depicted with brief explanations of their operating parameters. In general, the UAVs in Groups 2 through Group 5 are driven by gas powered motors while Group 1 aircraft are small, electrically powered systems.

Table 1. The Department of Defense unmanned aircraft system organization (from [3]).

UAS Category	Max. Gross Takeoff Weight (lbs.)	Normal Operating Altitude	Speed (KIAS)	Example Aircraft
Group 1	0-20	< 1,200 AGL	< 100	Puma, Wasp, RQ-11 Raven
Group 2	21-55	< 3,500 AGL	< 250	RQ-21A ScanEagle
Group 3	< 1320	< 18,000 MSL	< 250	STUAS, RQ-7 Shadow, MQ-5 Hunter
Group 4	> 1320		Any	A160T Hummingbird, MQ-8B Fire Scout, MQ-1C Grey Eagle, MQ-1B Predator
Group 5		> 18,000 MSL		MQ-9 Reaper, RQ-4A/B Global Hawk

UAVs are used for all missions, from intelligence, surveillance, and reconnaissance (ISR) to strike capable operations. These platforms provide an over-the-horizon or over-the-hill capability that is paramount to the warfighter. On the tactical level, the ability to organically establish reconnaissance and perspective of the battlefield is an integral advantage during wartime. It allows the commander to build a more accurate picture of the battle space without exposing his or her troops to enemy fire. During Operation Enduring Freedom, the use of UAVs was a proven combat multiplier, enabling troops to gather intelligence and root out the enemy while reducing the cost of human life [4]. In addition to the benefit provided to small units, UAVs can affect the theater and strategic level of warfare as well. Group 5 UAVs such as the MQ-9 Reaper are capable of precision strikes against enemy combatants and facilities across the globe. These actions act as anti-access and area denial systems [1]. In the future, the DOD looks to expand the use of unmanned systems and incorporate them into our existing defense infrastructure [1]. Such actions will serve to enhance the prevailing warfighting functions of the nation's military and enable them to respond to evolving technological threats.

As technology and the style of warfare evolve, the DOD anticipates that UAVs will enable a more rapid and effective response to future threats [1]. Expanding the abilities of the existing platforms then becomes an inherent requirement to meet the demands of that evolving threat. Currently, military UAVs are limited by the size of their payload and endurance. The current endurance for a UAV depends on the different payloads that it carries but can range from just over an hour for a Group 1 asset to 32-plus hours for the RQ4A/B Global Hawk [5]. While Group 1 platforms are an asset to the

warfighter, their dismal endurance and limited payload is a critical vulnerability. Fortunately, being driven by electric motors, those platforms are prime candidates for renewable sources of energy. As such, the incorporation of photovoltaic (PV) technology would extend the battery life of Group 1 aircraft and greatly increase the operating endurance and payload of the current systems.

B. RELATED RESEARCH

Previous theses at the Naval Postgraduate School have focused on the application of affordable thin film photovoltaic (TFPV) cells to a variety of aircraft platforms to demonstrate and model the extended endurance provided by this method [6], [7]. In this research, we expand upon the work started by William R. Hurd in 2009 with a model airplane [7] and most recently continued by Christopher R. Gromadski with an RQ-11 Raven in 2012 [8]. For a detailed background of solar flight and the different platforms in the UAV inventory, the aforementioned theses are available for further reference. In addition, the Air Force Research Laboratory demonstrated a 60% increase in flight endurance by utilizing thin-film, triple junction GaAs cells from MicroLink Devices in 2012 [9].

C. OBJECTIVE

It is a proven and worthwhile endeavor to increase the endurance of small Group 1 UAVs through the application of thin film photovoltaic (TFPV) cells [6]. The objective of this thesis is to investigate whether the highest efficiency $CuInGaSe_2$ (CIGS) cells, when applied to an RQ-11 Raven UAV, will power the aircraft from dawn to dusk and simultaneously increase the payload capacity. The possibility of applying TFPV cells to gas-powered UAVs in order to demonstrate the same result is also explored.

With recent advances in the efficiency and availability of CIGS cells, the affordability of previously unattainable assets is now logical with respect to the cost of a Group 1 UAV. It is important to this research that the solar cells applied to the aerial platform do not make the entire system cost prohibitive for the DOD. A cost benefit analysis demonstrates that higher efficiency TFPV cells are available but do not provide

the affordable and efficient systems sought by the current *Unmanned Integrated Systems Roadmap* [1].

D. APPROACH

In order to achieve the objectives, an actual RQ-11 Raven is ground tested in order to determine the power requirements for various throttle settings and individual payloads. Then, a modular solar array is designed and adhered to the wings of the Raven. Finally, the array and solar integrated UAV is tested in order to validate our predictions.

Information pertaining to the Raven's system characteristics, mission, and critical limitations is given in Chapter II. The photoelectric effect and the fundamentals of TFPV operation are reviewed in Chapter III. Next, solar cell parameters are defined and the design for the solar panel is presented in Chapter IV. Testing and analysis of the Raven system and solar panel are provided in Chapter V. Finally, conclusions regarding the potential of a solar cell integrated UAV are discussed in Chapter VI.

II. CURRENT ACQUISITION

A. RQ-11 RAVEN

As of mid-2013, there were more than 10,000 unmanned aerial systems across all the services, and the DOD has budgeted over 3.7 billion dollars for those systems in 2014 [1]. The vast acquisition of UAV platforms, especially Group 1 assets, is a testament to their battlefield utility and the drive for widespread application.

In this research we focus on the RQ-11 Raven, which is designed by AeroVironment and makes up the highest inventory of all DOD UAV platforms. It is a small, lightweight asset that is man portable and can be rapidly deployed for line-of-sight operations in day or nighttime environments with a range of 5.0 to 10.0 km. The system is easily hand-launched as shown in Figure 1. Weighing roughly 4.5 lbs with a 55.0 inch wingspan and a modular design, the aircraft and associated ground control equipment can be easily stowed and transported for expeditionary operations. The system is typically employed by a two- or three-man team [10]. However, the system is powered by a lithium ion (Li-ion) battery with an endurance limited to an advertised 60 to 90 minutes [11].

Figure 1. An RQ-11 Raven launch during Operation Iraqi Freedom (from [12]).

1. Mission

All Group 1 UAVs execute similar mission sets and are designed for small unit application. Their ability to be hand-launched and recovered in confined areas enables their use in isolated and austere operating environments, which precludes the reliance upon outside sources for battlefield intelligence and observation. Currently, most Group 1 UAVs are capable of autonomous operations with a constant Digital Data Link (DDL) to provide real-time video and data to the user. These capabilities enable them to conduct a variety of intelligence-driven missions that allow for remote reconnaissance and surveillance, force protection, target acquisition, and battle damage assessment [1].

2. System Configuration

Currently, the Raven system is composed of three Air Vehicles (AV), two Ground Control Systems (GCS), two payloads, a Reconnaissance, Surveillance, and Target Acquisition Kit, an Initial Spares Package, a Field Repair Kit, and a charger with multiple batteries for the AV and the GCS. As previously stated, the Raven system is designed to be completely modular in order to facilitate its use in austere environments. A breakdown of the AV components is presented in Figure 2. The wing is easily removed from the airframe and can be disassembled into three pieces. The tail boom, horizontal stabilizer, battery, and payload are all removed from the airframe as well. All the components of the AV fit within the man portable soft pack [11]. The GCS is also broken down and carried in a separate soft pack. The elements of the GCS can be found in [11].

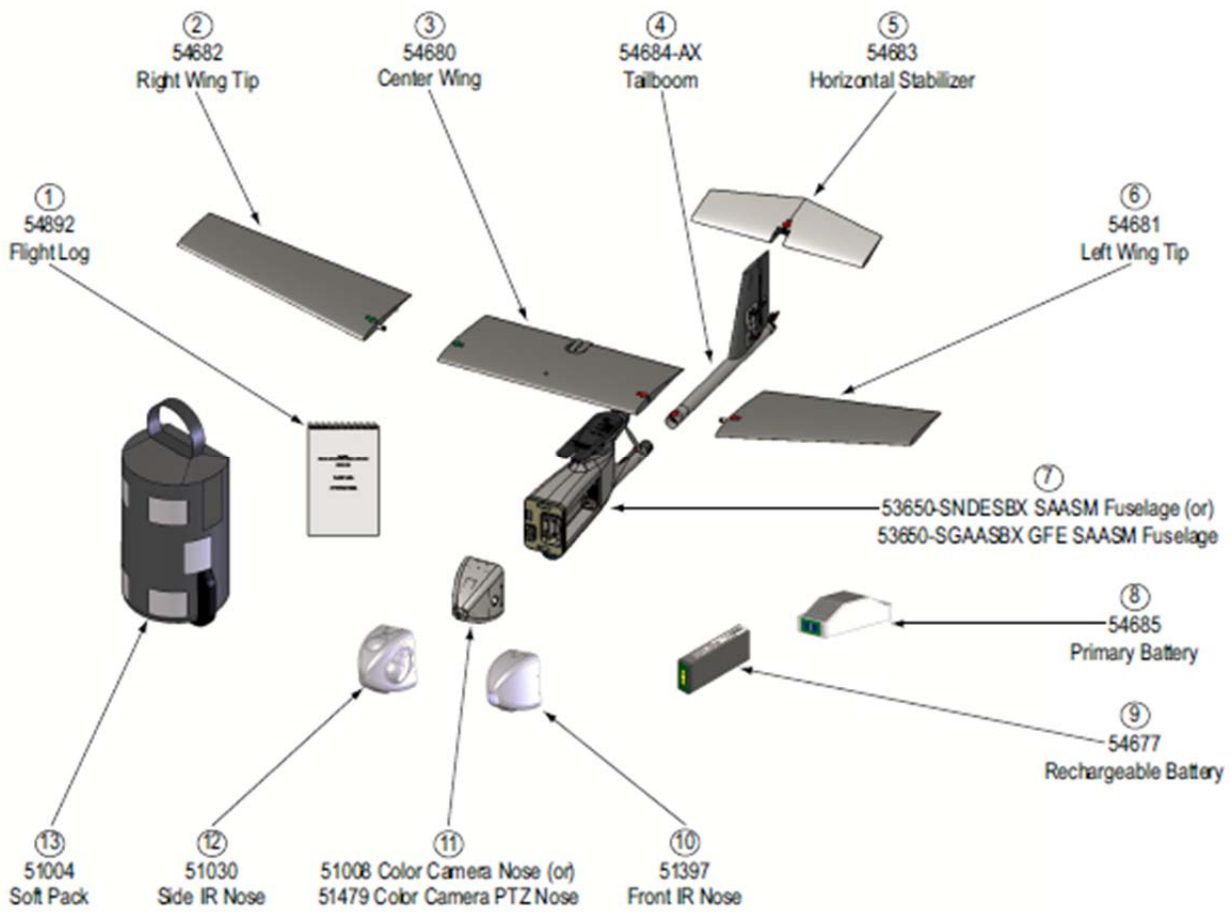

Figure 2. A breakdown of the RQ-11 air vehicle (from [11]).

3. Performance Characteristics and Limitations

The Raven utilizes a brushless direct current electric motor and is powered by a rechargeable 25.2 V Li-ion polymer battery with an advertised 98.0 watt-hours. The performance characteristics of the platform are summarized from the operator's manual in Table 2.

Table 2. The RQ-11 Raven operating parameters (after [11]).

Parameter	Characteristic
Wingspan	55 in.
Length	36 in.
Structure	modular, Kevlar Composite
Weight (W/Payload)	4.4 lb
Payload weight	6.5 oz
Normal Operating Altitude	150-1000 ft above ground level
Cruise Speed	26kts
Range	10km line of sight
Motor	Direct Drive electric
AV Batteries	Li-Ion (rechargeable)
Flight Duration	60-90 min
Launch	Hand Launch
Landing	Deep stall Autoland
Navigation	Global Positioning System and electronic compass
Flight Control	Manual or Autonomous
Windspeed	max 20kts
Rain	max 0.25in/hour

4. Payloads

The Raven system has experienced a series of payloads that have incrementally improved since its introduction to the fleet. Currently, AeroVironment advertises three different payloads to the consumer. These payloads are an electro-optical (EO) camera, an infrared (IR) camera with an IR illuminator, and a dual EO and IR camera mounted on a stabilized gimbaled payload [10]. The availability of a dual EO and IR payload is a vast improvement to the original system because it allows the operator to toggle between the two available payloads. However, a solar integrated Raven may be capable of generating enough power to run both payloads simultaneously, further enhancing the operator's capabilities.

5. Variants

The Raven that was used for research in [6] and [8] was an older model of the current platform. The initial model was produced up until 2006 and is known as the RQ-11A, or Raven A because of the analog communication system of the platform [13]. After 2006, the Raven B variant was released to the DOD with enhancements to the optics and guidance and control capabilities of the AV [13]. Shortly thereafter, the Raven B, DDL variant was announced, which employs all digital links to utilize bandwidth more efficiently. The DDL variant enables improvements to the cameras, allows for data encryption, and permits more AVs to operate within a set geographical area. Furthermore, the DDL version received an upgraded motor and speed controller "to provide more thrust and better power management" [14]. The difference in endurance between the variants is unclear and is part of the investigation of this research.

6. Comparable DOD Platforms

Other Group 1 UAVs that are candidates for solar integration are the RQ-12 Wasp and the RQ-20 Puma. These two platforms make up the majority of the existing DOD UAV inventory and are presented as a point of comparison. AeroVironment's RQ-12 Wasp, illustrated in Figure 3, is smaller in size and inventory compared to the Raven. It is a hand-launched system that one person can carry. While having similar operating characteristics and using the same ground control station as the Raven, the Wasp has only a 3.3-ft wingspan and weighs just 2.85 lbs. The endurance of the RQ-12 Wasp is limited to 50 minutes and a range of only 5.0 km [15].

Figure 3. An example of the Wasp UAV with a gimbaled payload (from [15]).

AeroVironment's dominance of the Group 1 UAV market continues with the RQ-20 Puma. Depicted in Figure 4, the Puma is significantly larger than the Raven and the Wasp, with a wingspan of 9.2 ft and a length of 4.6 ft. Still a man-portable platform, it weighs 13.5 lbs and boasts an endurance of approximately 3.5 hours over a range of 15.0 km. The Puma UAV is designed for both land and maritime operations and is launched by hand or an optional rail-launch system [16].

Figure 4. An example of the Puma UAV (from [16]).

7. Critical Limitations

While the advertised endurance of the Raven is 60 to 90 minutes, that endurance is subject to change depending on the operating conditions. In higher temperatures, the operator's manual warns that the flight time will be reduced [11]. Additionally, the battery charger is only capable of indicating the charge of the battery to within 10% of the actual voltage level. Therefore, while the charger may indicate that a battery is fully charged, it may not be. Additionally, if two drained batteries are charged simultaneously, the batteries will require a much longer time to charge in order to properly balance [11].

Furthermore, the burden of employing Group 1 UAVs is the extra gear that the warfighter is required to carry. The limited endurance and challenges of attempting to charge batteries in a battlefield environment encourages troops to carry more batteries into combat for redundancy. According to a report by the Naval Research Advisory Committee, in 2006 the average Marine carried a load of 97 to 135 pounds to combat. For such a staggering load, every ounce saved makes a significant difference [17]. With these systems, those additional batteries must be carried to ensure that a constant rotation

of aircraft can be launched and recovered to provide continuous coverage. The current endurance of the Raven is insufficient for small units to achieve continuous observation of an objective without cycling multiple aircraft and carrying additional batteries into combat. It is a critical shortfall of these platforms that must be addressed.

Similarly, the warfighter constantly seeks to expand the capabilities of current technology. The payloads of existing platforms are frequently expanded, but these improvements increase the power required to run them. So to meet these increases in power consumption, the payload capacity must expand to support the warfighter's growing needs. Existing systems must continue to evolve for the future operational requirements that are on the horizon. While the Group 1 UAVs fill an operational necessity that exists today, their capabilities must develop and improve to match the future threats to our national security. The *Unmanned Systems Integrated Roadmap* for 2013 charges that our current programs of record must "achieve the levels of effectiveness, efficiency, [and] affordability" to meet the demands of the next generation [1]. Alongside that imperative, the DOD budget is experiencing a reduction in the funding that enabled the acquisition of our current UAV assets. Ultimately, the military must continue to expand the technological capabilities of our current systems in a cost-effective manner [1]. A low cost, solar integrated UAV would increase both the endurance and payload capacity of our existing systems to meet these goals.

B. POTENTIAL COMMERCIAL AND OPTIMAL DESIGNS

1. Commercial Off-the-Shelf Technology

Perhaps a different design would provide the optimum candidate for a solar-powered UAV. An aircraft with more lateral surface area would benefit the most because it would harvest the most power from TFPVs. An array of UAVs outside of the DOD inventory match this requirement. In particular, some designs that sought to improve aircraft stability proved useful for solar cell integration. The Tango UAV produced by Draganfly Innovations in Canada has a tandem wing configuration that essentially doubles the useable surface area of the aircraft [18]. Advertised to improve stability and flight characteristics at low speeds, the Tango is shown in Figure 5.

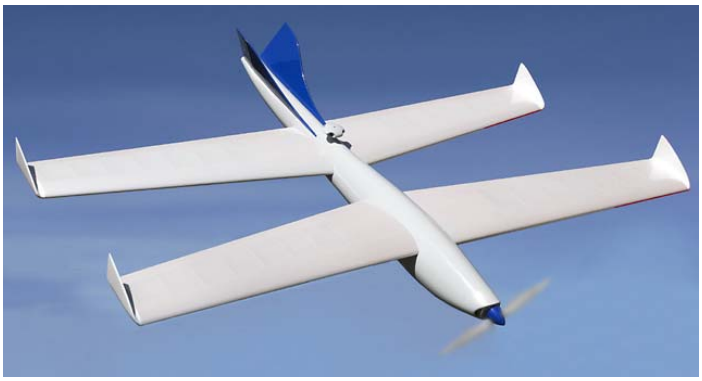

Figure 5. The design of the DraganFly Tango UAV (from [18]).

Similarly, Dara Aviation, based in Washington state, has a patented Joined Bi-Diamond Wing design for its D-1 models that reduces drag and increases lift. Like the Tango, the useable surface area is vastly increased by the unique design, which is shown in Figure 6. Additionally, the fuselage of this aircraft is also capable of solar integration because of its relatively flat and wide design.

Figure 6. The Dara Aviation lightweight UAV (from [19]).

These two aircraft designs are just two of the many available options in the commercial sector that might make for a better option for TFPV integration. Understandably, the acquisition process is slow and costly; therefore, it may not be a viable option for the DOD to invest in a whole new platform.

2. Modification of Existing Airframe

Previous thesis work by Javier Coba and Christopher Gromadski investigated the possibility of altering the airframe of the existing Raven in order to maximize the effect of solar cell integration [6], [8]. For their research, the expanded wing pictured in Figure 7 was designed and integrated with solar cells. A 70% increase in endurance was achieved with this method; however, flight tests were unable to be conducted. Nevertheless, the concept of altering the airframe begs the question of what other modifications would benefit a solar application. Potentially, the stabilizer could also be modified and used to contribute to the solar array. Additionally, the design of the tail boom could be altered to provide a flat surface that may also be utilized. In summary, a variety of alterations to the existing airframe would maximize the available surface area and contribute to the power generation of the solar array. However, maintaining the modularity of the system is critical to its introduction to the fleet. By creating a solid wing as in Figure 7, the concept was proven but more work must be done to show it does not preclude the expeditionary nature of the Raven system.

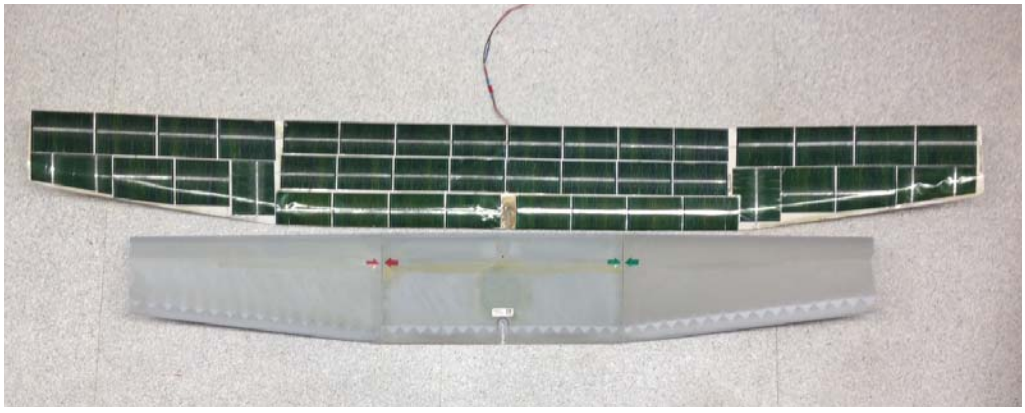

Figure 7. Comparison of the expanded Raven wing designed by [6] and the standard wing.

THIS PAGE INTENTIONALLY LEFT BLANK

III. CIGS PHOTOVOLTAIC CELLS

A. INTRODUCTION

More commonly known as solar cells, PV cells are designed and constructed with a variety of different materials and manufacturing methods. These subtle differences affect the conversion of solar energy into electricity and their ideal operating environment. However, the basis of all solar cells is the formation of a p-n junction in semiconductor material that acts as a reverse biased diode.

CIGS PV cells utilize another type of p-n junction called a hetero-junction that capitalizes upon the different semiconductor properties to achieve high solar conversion efficiencies. CIGS TFPV cells have made recent advancements in efficiency according to the National Renewable Energy Laboratory (NREL). NREL indicates that CIGS cells achieved a laboratory record efficiency of 20.8% in 2013 [20]; meanwhile, manufacturers advertise the ability to produce cells with efficiencies of more than 15% for the general public [21]. These TFPV cells are appealing because of their affordability with respect to their efficiency, as noted in Figure 8. While other TFPVs boast much greater efficiencies, their cost far exceeds the practicality of their application for the general consumer, including the DOD.

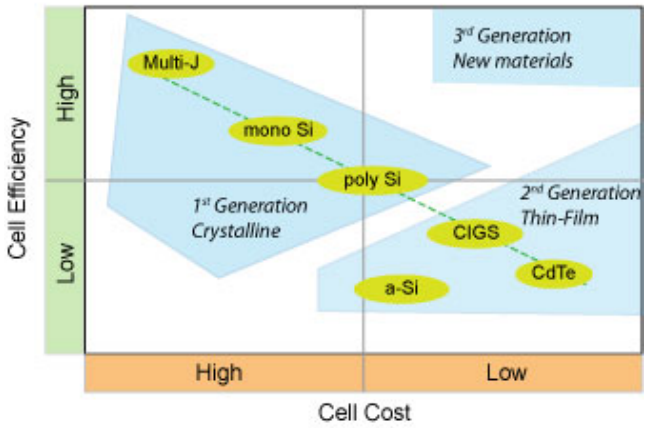

Figure 8. Cost versus efficiency in solar cell technology (from [22]).

1. Solar Radiation and the Solar Spectrum

The strength of the solar radiation on Earth is dependent upon a variety of factors ranging from atmospheric effects, latitude of the location, and the time of the year and day [23]. As solar radiation passes through the atmosphere, it experiences a reduction in power as a result of scattering and absorption by molecules and particulates in the air. Gasses have a tremendous effect on the absorption of photons because they have bond energies that are equivalent to specific wavelengths of light. The absorption and scattering caused by these gasses reduces the intensity of the light that ultimately reaches the Earth's surface as seen in Figure 9 [23].

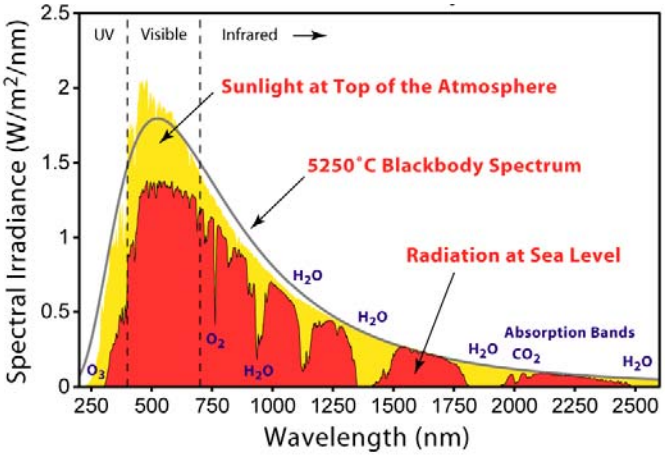

Figure 9. The solar radiation spectrum across a range of wavelengths (from [24]).

Outside the atmosphere, light has a solar radiation of approximately 1,367 W/m^2 [23]. To account for the absorption and scattering of photons, the path that light takes through the atmosphere with respect to the zenith is called the Air Mass (AM). On the Earth's surface, the solar radiation standard is AM 1.5 corresponding to a normalized solar radiation of approximately 1,000 W/m^2 [23]. An illustration of angular properties of Air Mass is presented in Figure 10.

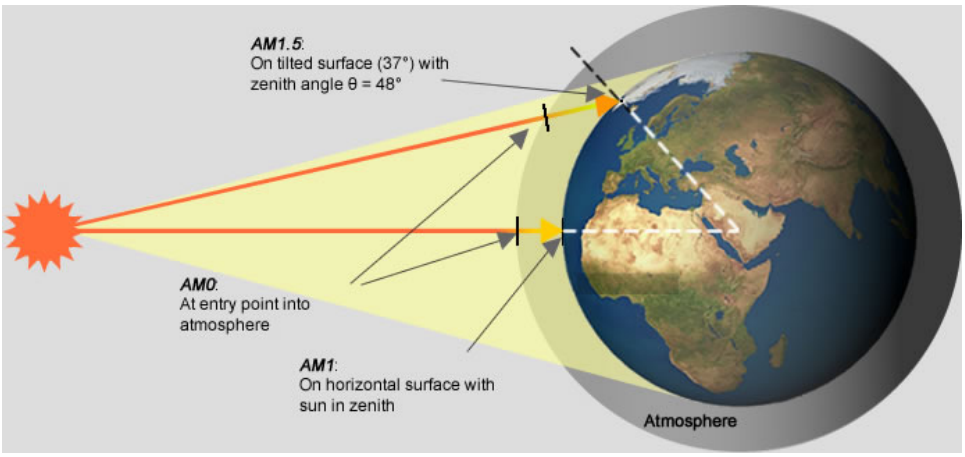

Figure 10. A depiction of the characteristics of Air Mass (from [22]).

2. Semiconductor Material and the Bandgap

Semiconductor physics enable the capture of solar radiation for conversion to electrical power. Every semiconductor has varying atomic structures that provide different properties utilized to elicit a unique PV response [23]. When multiple semiconductor atoms join together to form a crystalline structure, they are held together by the covalent bonds that exist between adjoining atoms.

Energy bands are determined by the allowable energy levels that an electron may occupy. In semiconductors and insulators, the valence and conduction bands are separated by a gap that grows wider as the strength of the bonds between atoms increases. In that gap, called a band gap, there are no allowable energy levels for the electrons. In order to achieve conduction, the electrons must receive enough energy to "jump" the band gap. In semiconductors, the bonds between atoms are readily broken, freeing up electrons capable of jumping the band gap to the conduction band. The movement of an electron from the valence band to the conduction band generates a hole, or the vacancy left behind by the electron. These holes are then filled by electrons from neighboring atoms. This process occurs throughout the material and once an electric field is applied, conduction will occur [25]. A graphical representation of the proximity between the conduction and valence bands is illustrated in Figure 11.

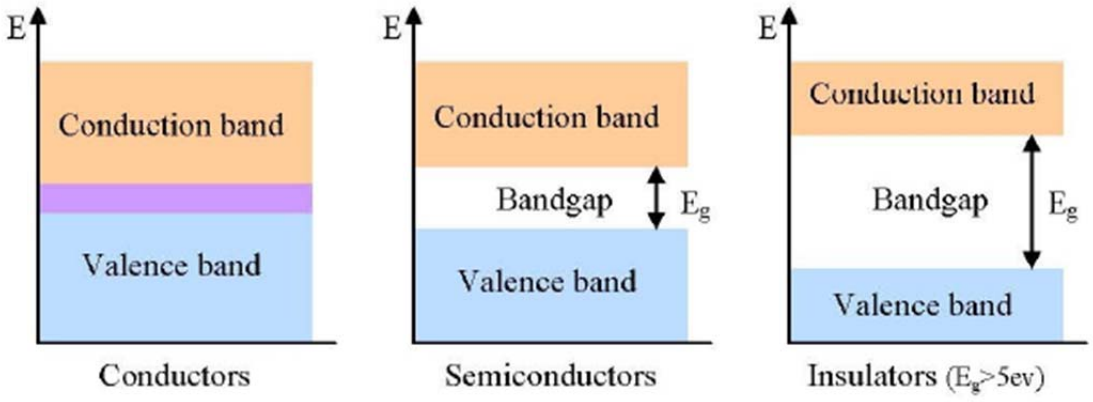

Figure 11. A comparison of the conduction and valence bands in a conductor, semiconductor, and insulator (from [26]).

3. P-N Junction

A material is considered n-type when it has a high concentration of electrons and p-type with a high concentration of holes. When p-type and n-type materials form a p-n junction, the majority carriers begin to diffuse from one side of the junction to the other. This movement is called diffusion. Due to the existence of diffusion current, an electric field of charged ions called the depletion region forms at the junction of p-type and n-type material. The potential of the electric field created is called the barrier voltage, V_O [26]. As a result of the exposed ions in the depletion region, a drift current develops that sweeps minority carriers from one side of the material to the other. When a kinetic particle, such as a photon, strikes an electron in the valence shell with sufficient energy to break the covalent bonds and jump the band gap, an electron-hole pair is generated. The electric potential of the depletion region then sweeps the electron to the n-type material and the hole to the p-type material, as seen in Figure 12. Ultimately, in a PV cell, the p-n junction is simply a reverse biased diode that maintains a voltage relative to the band gap of the semiconductor material [26].

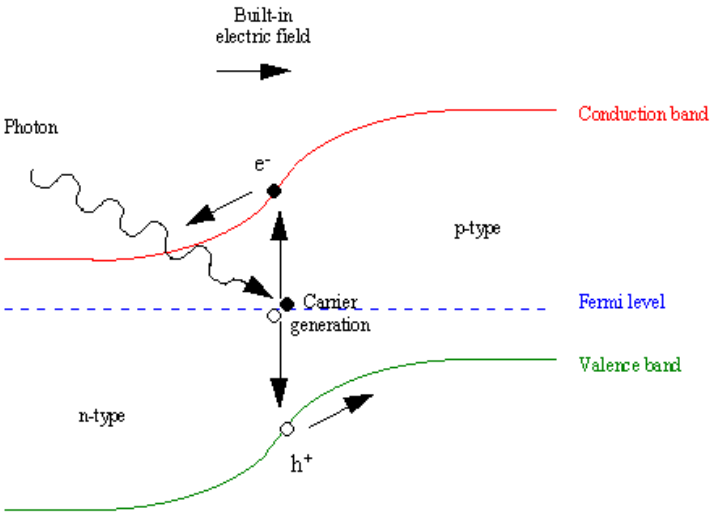

Figure 12. A demonstration of the photoelectric effect showing the Fermi level and carrier generation (from [6]).

Without collecting the electron-hole pair in a PV cell, the pair recombines before the two can be separated depending upon the mobility of the carriers and the diffusion length for the semiconductor. To form a solar cell, the current is harvested as electrons flow in the circuit from the n-type to p-type material [26]. The p-n junction is referred to as the absorption layer; the layer where electron-hole pairs are generated and separated. On top of the absorption layer, an anti-reflection layer permits light to pass through the cell and enter the p-n junction. Finally, on either side of the cell, ohmic contacts provide a path for the electrons and holes and feed the current to the load and prevent recombination within the semiconductor [26].

B. THIN FILM PHOTOVOLTAIC CELLS

1. Thin Film Silicon

Various manufacturing methods exist for creating TFPV cells depending on the desired efficiency or raw materials available. The basic silicon crystal (c-Si)-based TFPV cell structure is illustrated in Figure 13. A high-quality c-Si absorber is grown upon a seed layer. The absorber layer functions as the p-n junction of the cell. Then, the seed layer is applied to an inexpensive, flexible substrate. The efficiency of this type of PV cell depends greatly on the quality of the epitaxial layer of silicon and drives the

relatively high cost of these types of PV cells [27]. NREL has attempted to create c-Si cells with efficiencies near that of CIGS; however, this technology is also expensive and difficult to manufacture [27].

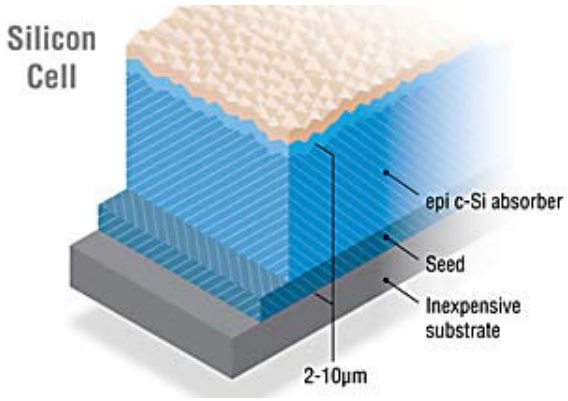

Figure 13. An example of the silicon solar cell structure (from [27]).

The more common type of Si TFPV cell is the amorphous silicon (a-Si) pictured in Figure 14. These cells are constructed with a transparent oxide followed by an absorber layer. The absorber is grown with an intrinsic Si layer in between p-type and n-type material. The intrinsic layer increases the electric field within the absorber layer and prevents recombination through drift current. As a result of its amorphous crystalline structure, the material is riddled with defects that decrease carrier mobility and increase the potential for recombination and traps [28]. Ultimately, the efficiency of these TFPV cells has plateaued over the last decade at roughly 13% [28].

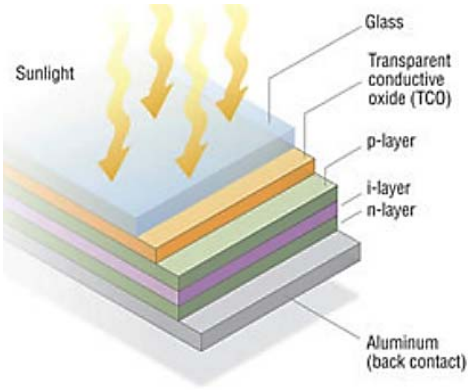

Figure 14. An example of the amorphous silicon cell (from [28]).

2. CIGS

CIGS construction is based on a different concept than the traditional, Si TFPV. By utilizing different semiconductors to create a p-n junction, the CIGS cell is considered a heterojunction. CIGS were created as a low cost alternative to the traditional solar cell because both the manufacturing process and the materials are cheaper in comparison [29]. A typical CIGS cell is presented in Figure 15. Photons enter the cell through a high band gap zinc oxide layer before passing through an n-type Cadmium-Sulfur (CdS) buffer layer. The absorber layer is comprised of a p-type CIGS layer that forms a p-n junction with the CdS buffer. These layers are then deposited upon a substrate that can be either rigid or flexible, depending upon the desired application [29].

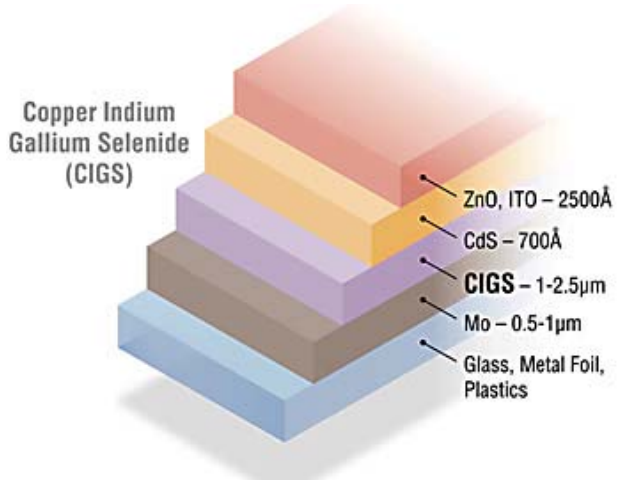

Figure 15. The structure of a copper indium gallium selenide solar cell (from [30]).

The absorber layer is traditionally made with $CuInSe_2$; however, the introduction of Gallium increases the band gap of the material closer to 1.4 eV which is considered the optimal band gap for the solar spectrum. CIGS is also a direct band-gap semiconductor and the majority of light is absorbed close to the p-n junction, reducing the chances of recombination within the absorber layer [29]. Additionally, the CIGS layer is a forgiving material with respect to defects in the lattice structure which reduces the cost associated with purification of the semiconductor material [29].

3. Cadmium Telluride

Similar to CIGS, Cadmium Telluride (CdTe) cells are based on a hetero-junction of two different semiconductors that form a direct bandgap of 1.45 eV. CdTe cells are lower in material and manufacturing costs; however, the toxicity of Cd can be a deterrent to some consumers. Additionally, the careful doping of Gallium required for CIGS is unnecessary with CdTe. The cells are constructed with a glass layer on top of a transparent conductive oxide that acts as the top contact. Next, a large band gap, n-type layer of Cadmium Sulfide forms a p-n junction with a layer of p-type CdTe. All of these layers are deposited upon a metal contact as seen in Figure 16 [28]. The efficiencies of CdTe cells in the laboratory have made substantial gains in 2013 and are vying with CIGS for the top contender in the TFPV market [30].

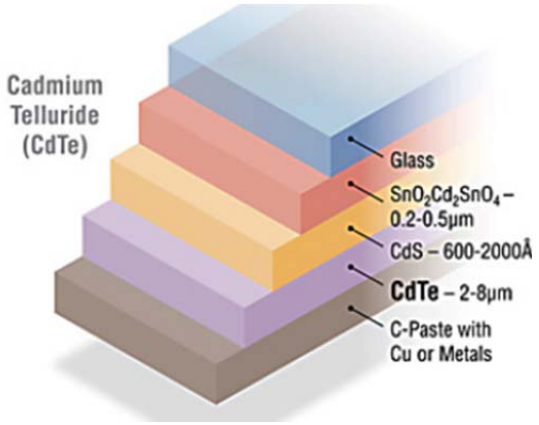

Figure 16. The structure of CdTe solar cell (from [30]).

IV. POWER INTEGRATION AND SOLAR ARRAY DESIGN

In order to incorporate a solar array into the existing power infrastructure of the Raven AV, a power converter, maximum power point tracker (MPPT), and balance charger are required. The power converter boosts the output of the array to the appropriate voltage for the AV, while the balance charger ensures equal charging of the individual Lithium cells of the battery. The MPPT uses an algorithm to maintain the greatest fill factor and efficiency possible as the power fluctuates due to external influences.

Two different solar array designs are presented that explore various possibilities for CIGS integration. The first utilizes the standard-size wing with modular properties, and the second is for an extended center wing from [6]. Both designs are compared to demonstrate the difference in power generation based upon the efficiency of the CIGS installed.

A. SOLAR CELL PARAMETERS

In order to evaluate a PV cell, the open circuit voltage V_{OC}, short circuit current I_{SC}, and efficiency η are used to characterize its performance. The fill factor indicates the difference between the measurable power of a cell compared to its theoretical potential. To determine that potential output, V_{OC} is measured when the p-n junction has reached equilibrium. This value is equivalent to the voltage drop of the diode formed by the p-n junction. Conversely, I_{SC} is the maximum current of the PV cell when the p-n junction is shorted. Those two parameters form the solid line of the IV curve in Figure 17.

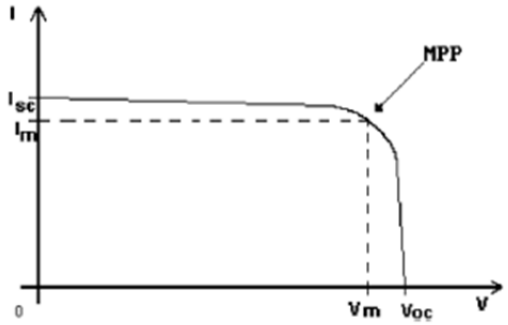

Figure 17. A typical IV curve for a PV cell (from [31]).

The intersection of I_m and V_m in Figure 17 is called the maximum power point and determines the efficiency of the array. In order to ensure operation at that point, an MPPT is required. The efficiency of the PV cell is determined by

$$\eta = \frac{P_{out}}{P_{in}}, \tag{2}$$

the output power of the array compared to the input power of the photons striking the surface. Therefore, the input power is dependent upon the wavelength and air mass of the incident light. Meanwhile, the fill factor is determined by

$$FF = \frac{I_M V_M}{I_{SC} V_{SC}}, \tag{3}$$

the ratio of the measured voltage and current at the maximum power point with respect to I_{SC} and V_{OC}.

1. Performance Factors

Myriad factors degrade the performance and efficiency of PV cells. To maximize the efficiency a cell, semiconductor physics, photon reflection, texturing, lattice structure, layer depths, and contact widths are just a few of the aspects that must be accounted for when designing PVs. For more information on these factors, [32] offers a detailed analysis. The aforementioned aspects are outside the scope of this research and the stated objective; instead, those factors affecting a solar-integrated UAV are addressed. A solar UAV is affected mostly by variations in the angle of incident light, temperature, and the solar irradiance of the operating environment. These characteristics dictate the fill factor

of a particular cell's IV curve. They shift the maximum power point and have the greatest effect on the performance of PV cells, as seen in Figure 18 [32].

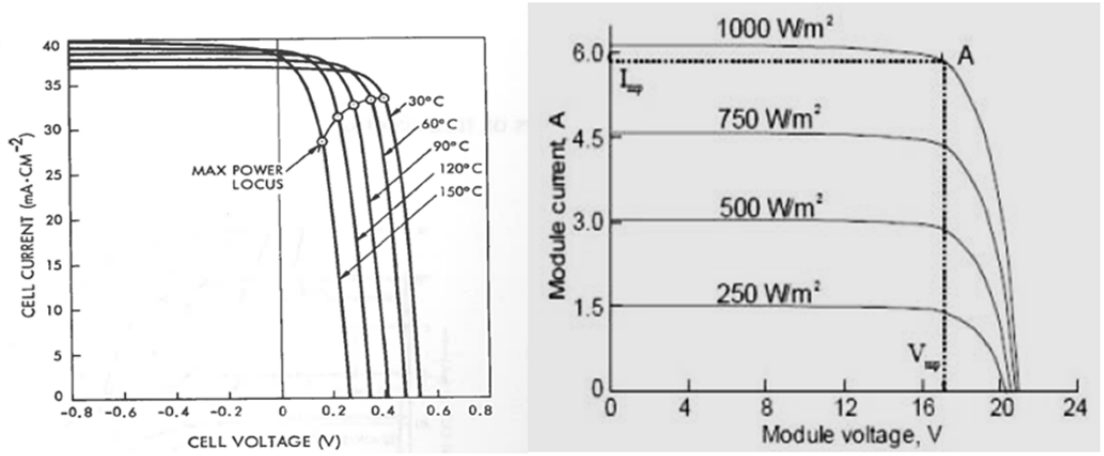

Figure 18. The effect of incident sunlight and temperature on output current and voltage (after [32]).

B. POWER INTEGRATION

1. Maximum Power Point Tracker

An MPPT is required to maximize the output of the solar array as the voltage and current vary due to external influences. The MPPT shifts the operating point of the solar array in order to provide the most power to load. It does this by continuously monitoring the current and voltage of an array at a fixed sampling frequency. Calculating the power for each sample, we find that the MPPT adjusts its relative impedance to match the impedance of the array in order to maintain operation at the maximum power point [33]. Utilizing the example in Figure 19, we see that if the solar array is connected directly to a 12.0 V battery through a conventional controller, the output power is limited to 53.0 W. Conversely, an MPPT matches the resistance of the load to calculate the optimal voltage in order to produce the highest power from the solar array. When the MPPT is utilized, the array produces the full 75.0 W available in the example [34]. Since the voltage output of the array will be either higher or lower than that required by the load, a DC-DC converter will ensure that the voltage supplied to the load is regulated to the proper amplitude.

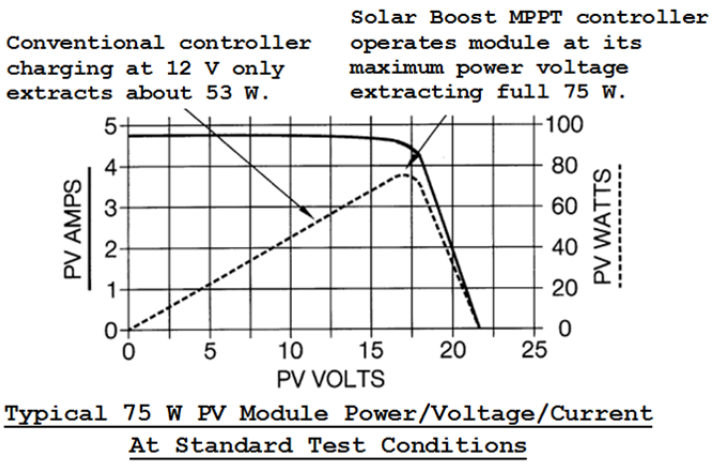

Figure 19. The basic operation of an MPPT (after [34]).

2. DC-DC Power Conversion

The output of the PV array cannot be directly applied to the existing power infrastructure of the Raven AV because it is unregulated. In order to integrate the array, a DC-DC power converter must boost or buck the voltage to the appropriate level of the battery. For the design in this research, the output voltage of the array will not be greater than the battery voltage, as is discussed in later sections. Therefore, a boost converter is the appropriate device for integration with the Raven. In Figure 20, the basic schematic of a boost converter is presented. With the switch in the closed position, the diode is reversed biased, isolating the output from the input. Meanwhile, the capacitor maintains the existing voltage of the load on the output. In the open position, the output receives power from the combination of the inductor and the input which is fed directly to the load and charges the capacitor [35].

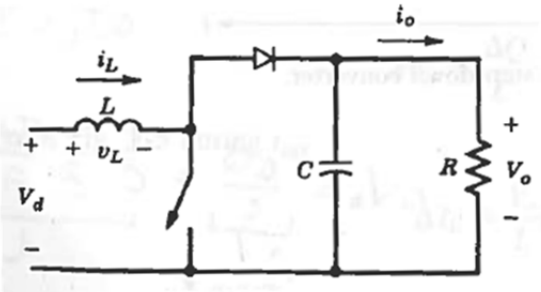

Figure 20. A basic boost converter schematic (from [35]).

The output voltage of a boost converter is controlled by the duty ratio *D*, representing the amount of time the switch is on with respect to one period of the switching cycle. The output voltage is then determined by

$$V_{out} = V_{in}\left(\frac{1}{1-D}\right). \tag{4}$$

3. Balance Charger

Finally, after the MPPT and DC-DC converter, a balance charger is the last power component separating the battery from the array. A balance charger decreases the risk of fire due to overcharging, a risk inherent to all Li-ion batteries [8]. Since the lithium battery of the Raven comprises multiple cells that discharge unequally during operation, a balance charger ensures that each individual cell is charged appropriately. For example, the Ultra-Balancer selected by [8] and utilized in this research continuously monitors the voltage of each cell in the battery and prevents any cell from charging faster than the others. When a cell voltage is higher than that of adjacent cells, it is discharged with 150 mA current until the voltages are equal [8].

C. SOLAR ARRAY

1. Design

Integral to the future acquisition of a solar integrated UAV is the modularity and portability associated with the current model. In order to maintain those characteristics of the Raven, a modular wing design is presented. Capitalizing upon the existing fasteners used to bind the three sections of the wing, we incorporate the positive and negative leads of the solar array into these connections for ease of integration. The existing fasteners are made of aluminum and do not allow for proper conduction. In order to ensure both an effective connection between wing sections and a durability to last multiple missions, the fasteners were redesigned. Installation procedures for the redesigned fasteners are located in the Appendix. This concept is shown in Figure 21 with an example connector to use for the wing interface.

Figure 21. An example of the connector used to connect the wing sections.

The standard wing of the Raven measures 2359.9 cm^2 when treated as a single entity like the extended wing in [6] and not three different sections. Adjusted for the placement of CIGS which requires a small portion of the area for leads and thin spaces between cells, the effective area of the wing is approximately 1943 cm^2. If CIGS are manufactured specifically for this wing, more of the theoretical area may be utilized. The dimensions of the CIGS used for this research were a limiting factor and as such, only 40 cells were installed on the wing as shown in Figure 22.

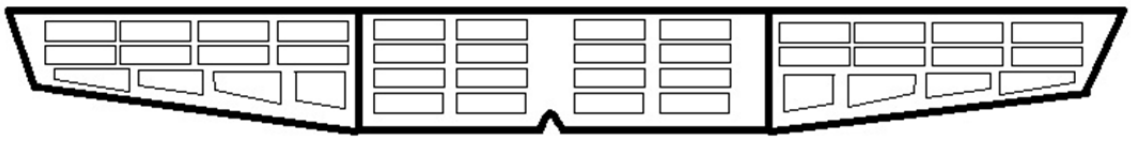

Figure 22. The solar array design for the standard Raven wing.

The array can be constructed in series to maximize the voltage potential or parallel to increase the overall current. Choosing a series connected array for this design, the voltage output of the array is highest at a potential 19.0 V; however, the current is limited by the cell with the lowest current. The potential power produced under standard test conditions (STC) from this wing compared to the efficiency of the CIGS utilized is presented in Table 3. STCs assume operation under AM1.5 at 25.0 C. Power calculations were determined from

$$Power = \left(1000\frac{W}{m^2}\right)(0.1943m^2)(\eta). \tag{5}$$

Table 3. The power output of a standard wing design for various efficiencies.

Efficiency of CIGS	Theoretical Power
10%	19.4 W
15%	29.2 W
20%	38.9 W

The modified wing in [6] was also series connected with an effective surface area of 3180 cm^2 for an expected output power of 29.6 W. However, once constructed and tested in the Monterey Bay Area of California, the output power of the solar array measured between 10.0 and 14.0 W due to environmental factors and losses in the power circuitry. As a result of the elongated wing, engineers witnessed a 37% increase in flight endurance and [6] demonstrated that an additional 20 to 70% increase in battery life is possible due to the solar array. The output power of an equal sized array with CIGS of varying efficiencies is calculated by (5) and presented in Table 4.

Table 4. The power output of a modified wing for various efficiencies.

Efficiency of CIGS	Theoretical Power
10%	31.8 W
15%	47.7 W
20%	63.6 W

THIS PAGE INTENTIONALLY LEFT BLANK

V. TESTING AND ANALYSIS

Prior to any testing of a TFPV array, the Raven AV was tested to establish a baseline for all future measurements. The modular solar array was then constructed and the power generation was measured under various conditions. Finally, the array was integrated with the Raven AV, and the measurements were repeated to determine any differences from the baseline. All tests and measurements were conducted in a laboratory environment and the AV was not flown.

For data collection, the LabVIEW program was utilized to record all data measurements. This program interfaces directly with a dual display multimeter in order to simultaneously record both current and voltage dependent upon a user defined sampling frequency. The LabVIEW data files used were those first coded in [6]. A basic schematic of the lab set up is presented in Figure 23.

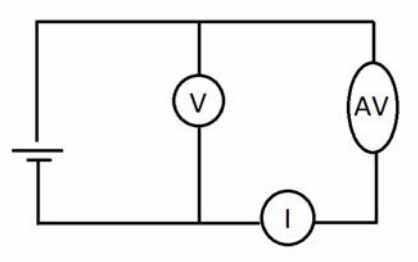

Figure 23. A basic schematic of the test setup.

A. SYSTEM TESTING AND CALCULATIONS

1. System Configuration

In order to determine the increase in endurance and payload provided by the array, a baseline must first be established. To accomplish this task, the power consumed by the Raven was determined over a range of throttle settings with five different batteries and three AVs. The average current at each throttle setting is an indicator of how much power a TFPV array must produce to replace the Li-ion battery during flight.

The rechargeable Li-ion polymer battery for the Raven system is depicted in Figure 24. Along the top surface are positive and negative leads that interface with the AV circuitry when inserted in the fuselage. The thin strip of connection ports along the edge of the battery are used for charging purposes only and provide access to the individual cells to ensure a balanced charge. At a full charge the battery measures 25.2 V with a capacity of 3.9 A-hours. During operation, the GCS displays a low battery voltage warning when it detects the battery voltage is at 21.9 V, an indication of 10 to 15 minutes of flight time remaining. The Raven system automatically lands the AV if the battery reaches an extreme low voltage of 19.0 V [11]. This emergency procedure protects the AV because as the voltage of an individual Li-ion cell drops below a lower threshold of approximately 3.0 V, it permanently damages the cell and limits the capacity of the entire battery [8].

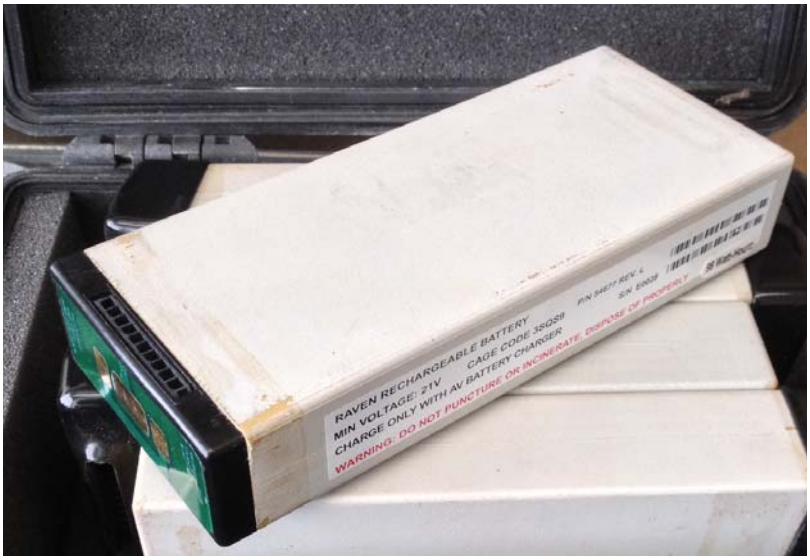

Figure 24. The RQ-11 Raven rechargeable lithium ion battery.

2. Power Consumption

Current draw is an indicator of the power drawn by the aircraft in each throttle setting. According to [36] and [11], the AVs throttle is set to 100% to achieve the desired operating altitude, typically between 100 and 300 ft [37]. With a climb rate of 800 ft/min, the operator is expected to achieve the proper altitude within 20 s [11]. In

order to maintain altitude during flight, a typical throttle setting is between 50% and 55% [36]. In order to lower the altitude, a 45% throttle is commanded and for a climb a 65% throttle is utilized. However, [36] indicated that Raven operators are instructed to place the aircraft in an autonomous mode during a mission. In this mode, the operator does not control the throttle. The AV automatically adjusts the amount of voltage and current drawn from the battery in order to maintain an airspeed of 26 knots at the commanded altitude. Whatever power the AV draws in this mode is not displayed or recorded for the operator. Therefore, for this research a throttle setting of 100% is commanded for 20 s to simulate the climb to operational altitude followed by a setting of 50% to approximate the power required to maintain altitude during the preponderance of a typical operation. The set up for this period of testing is displayed in Figure 25.

Figure 25. The set-up for the baseline testing of current draw and endurance.

To start, the current at each throttle setting was determined with multiple measurement devices, AVs, and batteries to produce the average current values presented in Table 5 and graphed in Figure 26. Previous research from [8] is also plotted in Figure 26 for comparison.

Table 5. The average current of the Raven AV at different throttle settings.

Throttle	Current (A)
0%	0.62
25%	1.23
30%	1.40
35%	1.64
40%	1.96
45%	2.29
50%	2.79
55%	3.42
60%	4.19
65%	5.08
70%	6.32
75%	7.75
80%	9.58
85%	11.61
90%	14.36
95%	15.97
100%	18.25

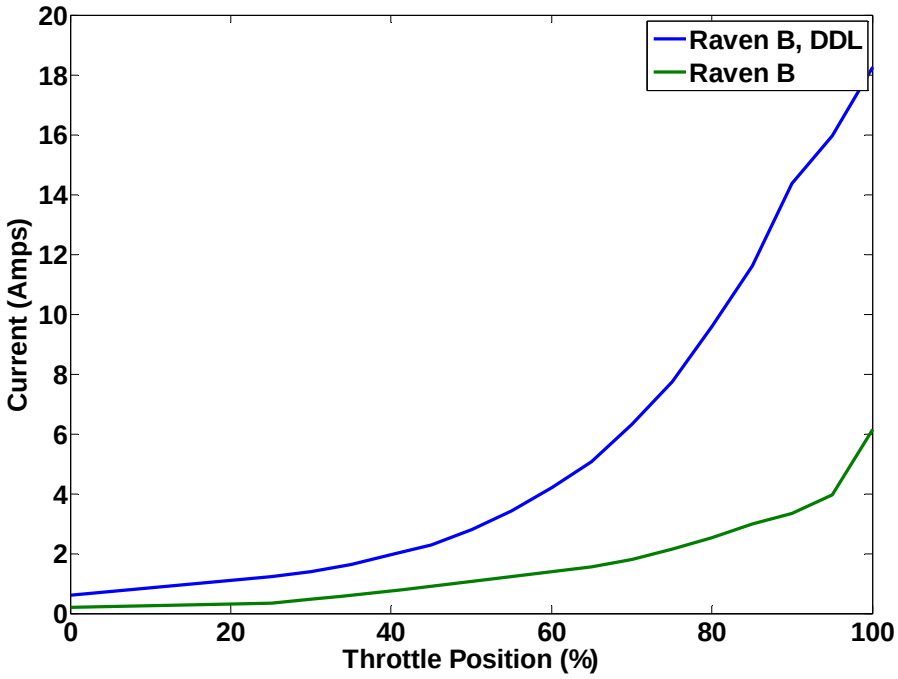

Figure 26. Average current draw of the Raven B, DDL variant at multiple throttle settings compared to the Raven B data (from [8]).

The relatively large magnitudes of current were alarming because they are greater than the measurements recorded and utilized for simulations in [6], [8], and [38]. After further analysis, it appears that the Raven A and Raven B drew far less current than the Raven B, DDL variant. These differences render the benefits predicted by previous research void and require a whole new set of simulations and calculations to account for the higher power requirements of the enhanced digital system. To eliminate the batteries as a source of error, PMA-263 provided an additional complement of batteries, but the test results remained consistent. It is possible that the three AVs utilized for this research have higher power requirements due to long term storage effects or previous damage. Further research is required to confirm whether or not the AVs utilized are an anomaly or are indicative of a full mission capable Raven. Nevertheless, the power requirements measured in this portion of the research are utilized as the baseline parameters for the remaining analysis.

3. Average Endurance

The average endurance was determined by conducting a ground test of the AV with a throttle setting of 100% for the first 20 s followed by a setting of 50% until the GCS indicated the battery voltage reached 21.9 V. This testing procedure was repeated with two different AVs and five different batteries to determine an average endurance of 29.97 minutes presented in Table 6. The total mission time of 44.97 minutes can be calculated by adding 15 minutes to account for AV retrograde. Averaging approximately 45 minutes, the total mission time observed in the baseline tests is consistent with what [36] predicted based on his experience with the Raven B, DDL. The results of the battery voltage endurance tests are also presented in Figure 27. These times are significantly shorter than [8] and [6] but are consistent with the current draw measurements in the previous section. One cause for the difference between this research and previous work is the interpretation of the AV voltage. For these tests, the voltage transmitted by the AV and displayed on the GCS was utilized to determine the end of each measurement. Conversely, in [8], the voltage indicated on the voltmeter was used to determine the conclusion of the test. This subtle difference accounts for upwards of 20 to 30 minutes of flight time because the voltage indicated by the multimeter was approximately

0.3 V greater than the voltage reported by the AV. Nevertheless, despite this procedural difference, the endurance of the Raven B, DDL is significantly shorter than the analog Raven as illustrated in Figure 28.

Table 6. The average endurance and power requirements of the Raven B, DDL operating at 50% throttle.

Test	Time (min)	Average Power from Battery (W)
1	22.90	72.19
2	27.50	71.39
3	32.50	69.91
4	30.92	70.18
5	30.32	69.35
6	35.70	69.36
Averages	**29.97**	**70.40**

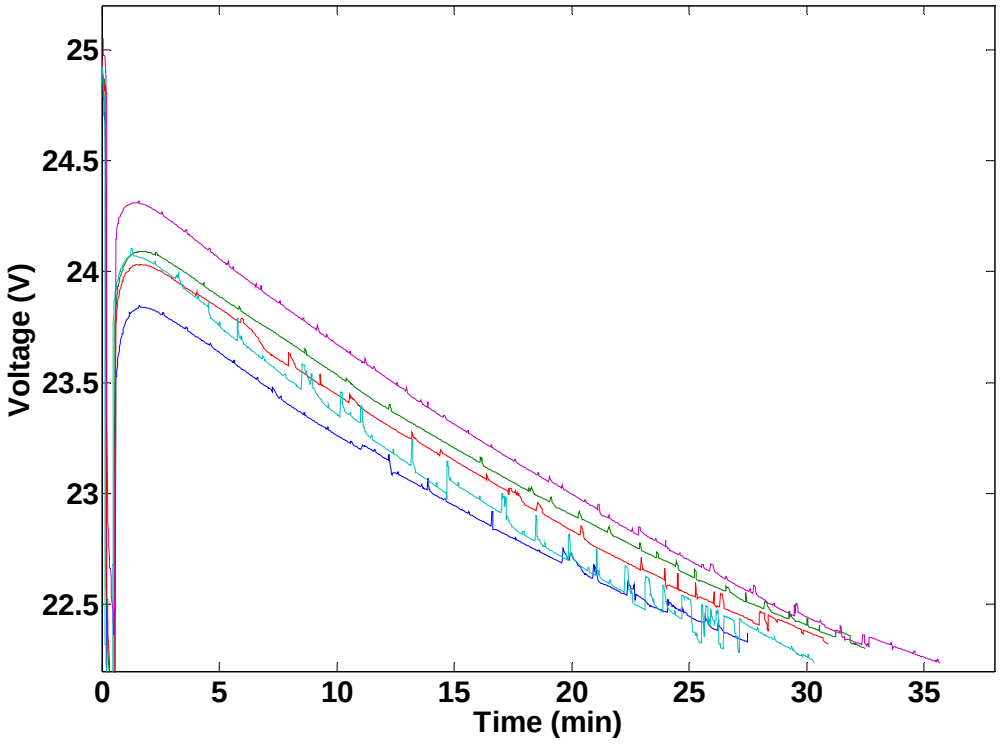

Figure 27. The results of the Raven B, DDL battery voltage endurance tests.

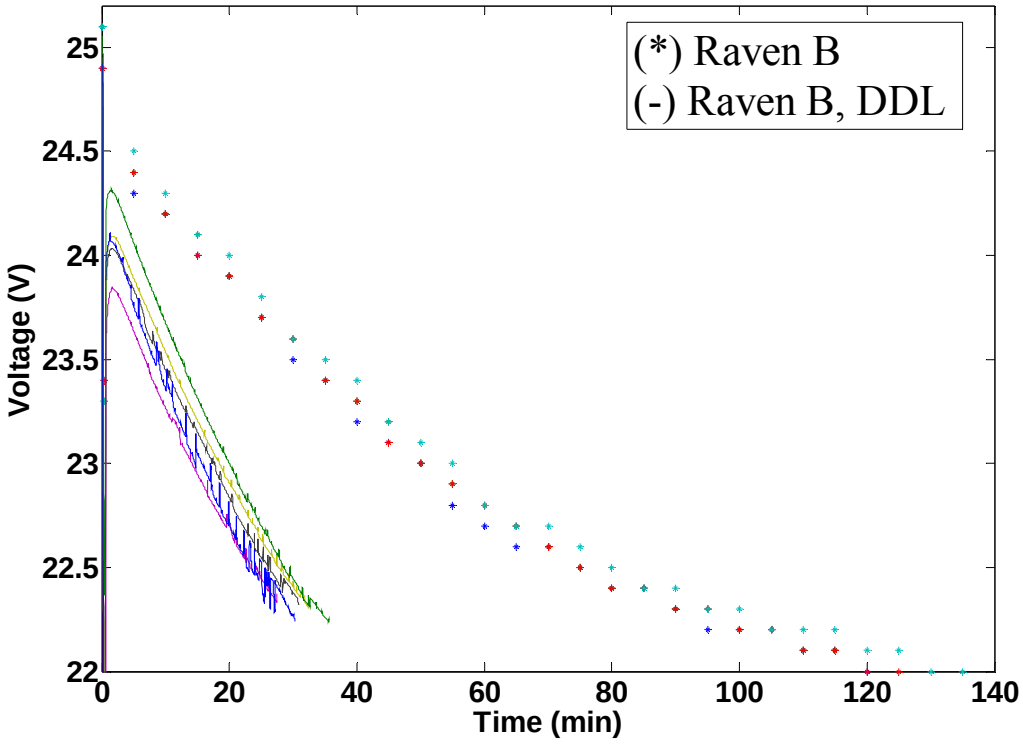

Figure 28. A comparison of the battery voltage endurance tests for the Raven B and Raven B, DDL platforms (from [8]).

Furthermore, the average power required to maintain a 50% throttle position was 67.0 W; however, the peak power at 100% throttle averaged 381.0 W. By comparison, the power consumed by [6] at 55% throttle was approximately 30.0 W, less than half the power required for the Raven B, DDL. In summation, baseline testing confirms that the Raven B, DDL variant of the RQ-11 has a shorter endurance and higher power requirements than the analog Raven variant used for testing in [6], [8], and [38].

B. PAYLOAD TESTING AND CALCULATIONS

Analyzing the connection port used for the AV to interface with the EO and IR payloads, we measured the voltage and current draw of those payloads. To determine the voltage provided to the payload, a voltmeter measured the electric field potential of the connection port while the AV was running. The current drawn by the EO and IR cameras was determined by monitoring the device through the LabVIEW program as the payloads

were disconnected, installed, and run through the full gambit of operation. The results of this experiment are displayed in Figure 29.

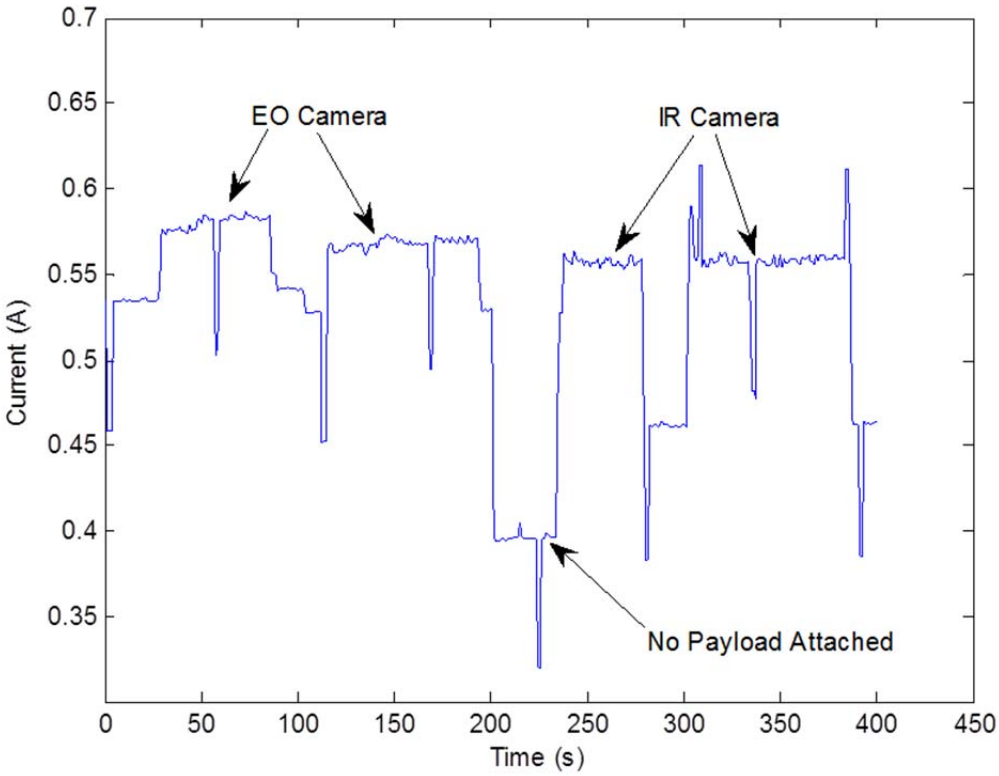

Figure 29. The current measurements used to determine payload power requirements.

While disconnected from the AV, the connection ports of the interface indicated a maximum voltage of 16.0 V is supplied to the payload. The current drawn from the battery and supplied to the AV in this configuration was 0.395 A. To determine how much current was directed to the payloads, the EO and IR cameras were attached, and the difference indicates the amount of current that is required to operate the respective payloads.

There are multiple settings for the EO payload that the user can choose. Selecting the front or side look camera, the user can then set the zoom level of the payload. Furthermore, the user has the option to view the camera in a filtered mode that reduces over-exposure. Toggling through the various settings of the EO payload, the highest

current draw was measured at 0.587 A while the camera was in the side look mode at the highest zoom level. With the IR payload attached, the user may select black-hot or white-hot modes of operation. Additionally, the user can toggle the IR illuminator. The current was relatively constant for every setting of the IR payload and peaked at 0.564 A.

From these data it was determined the EO camera requires 187.0 mA for operation while the IR camera draws slightly less current at 164.0 mA. Accounting for the voltage measured at the interface of the payload and the AV, we see that the payloads require anywhere from 2.62 W to 2.99 W for normal operation. Considering that the measured values do not represent the limitations of the payload, it is assumed that a margin between continuous and peak current is accounted for in the design. For this reason, to consider an alternative power source for the payload, we assume that a solar array must be capable of providing a continuous power of 6.0 W and handling more in power surges.

The solar array designed in Chapter IV for the standard wing of the Raven AV has a theoretical power output of 19.0 W for low efficiency CIGS of 10%. This power output is a promising alternative for operating the current payloads of the Raven B, DDL variant and for future, more demanding payloads.

C. SOLAR ARRAY TESTING

1. Final Modular Array Construction

To maintain the modular design of the Raven, commercial power cables were chosen to replace the wing pin and wing cup that connect the three portions of the wing. After purchasing a variety of different cable assemblies, cable part number 839-1173-ND from DigiKey was selected for the design because its shape closely matched the dimensions of the existing fasteners. Next, the instructions for the removal of the wing pin and wing cup were found in the 2008 edition of the *Raven B Small Unmanned Aerial System Intermediate Level Repairs Manual* [39]. Following those instructions, the wing pin and cup were removed from the three wing sections. A drill was then used to expand the remaining holes in the wing to accommodate the power cables. Small holes were also drilled into the underside of the wing to provide access to the leads of the cable. Lastly,

an epoxy was used to ensure that the leads were firmly seated in the wing. The final product is displayed in Figure 30.

Figure 30. The installation of the cable assembly in place of the wing pin and wing cup.

Once the wing pin and cup were installed, construction of the solar array began. The CIGS utilized for the array were from Global Solar Energy, the same cells used in [6]. Unfortunately, the CIGS had most likely degraded from the 13% efficient cells they once were due to oxygen exposure and handling over time. Without the ability determine efficiency with a solar simulator, the efficiency was estimated to be between eight and ten percent. Despite the reduction in efficiency, the CIGS were still expected to provide a significant amount of power to both expand the payload capacity and endurance of the Raven B, DDL.

The procedures for handling, cutting, and sealing the array from [6] and [8] were used to construct the array in this research. The CIGS utilized for the array were not encapsulated and were arranged in a series connected sheet of 18 cells. Each individual cell was 10.0 cm long by 21.0 cm wide. For the array design in Chapter IV, 40 solar cells needed to be fashioned from the series connected string to adhere to the wing sections. The cells on the center wing were cut to approximately 45.0 cm^2, while the side wings

had cells that were 50.0 cm^2. It was assumed that the current would be slightly lower in the side wings because they would not directly face the sun; therefore, the cells on the side wings were larger to account for the angle of incidence with the sun and increase their current production.

During construction, it was discovered that cutting the CIGS across the center busses proved both challenging and detrimental to the output of the solar cell. As a result, the design in Chapter IV was modified to reduce the number of cuts and solder connections required to build the array. This design change reduced the overall number of CIGS to 38 series connected cells but proved to be a more efficient method of construction. Once the CIGS were cut to the proper dimensions, they were all tested individually to ensure they were not damaged. First soldered together and tested on a workbench in the appropriate design, the solar cells were then applied to the surface of the wings. Double-sided tape held the cells in place while common packaging tape was used to encapsulate the CIGS on the wing. As predicted by the test results in [6] and [8], a boost in performance was witnessed after the CIGS were encapsulated.

Next, the leads of the array were soldered to the power cables that were previously installed in the wing. Copper tape was used to both hold the leads in place and ensure a conductive path for the current. Since it was known that this prototype would not be used in flight, measures were not taken to reduce the effects of the exposed leads on the aerodynamics of the airfoil. In application, these leads can be recessed into the wing and sealed to guarantee a smooth surface. Additionally, as a result of the power cables chosen, the side wings did not sit flush with the center wing. In future applications, a more suitable connector may be chosen that will enable the wings to mate properly with one another. The final array is presented in Figure 31.

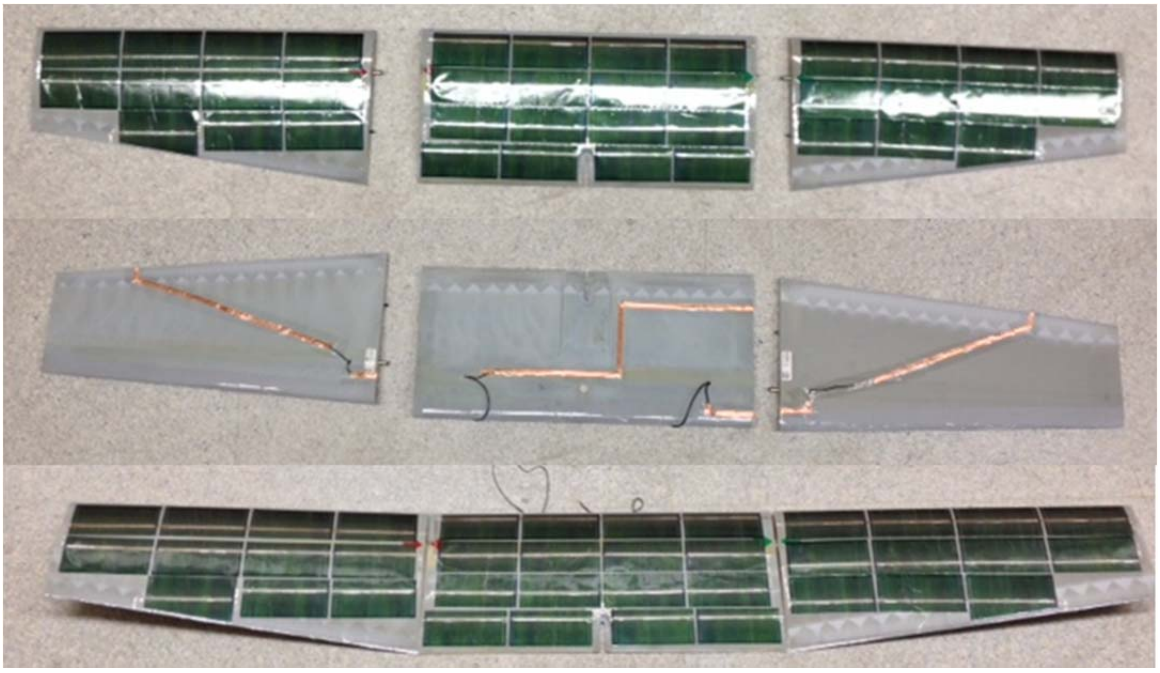

Figure 31. The final array demonstrating the wing's modular properties.

In total, a surface area of 1,828 cm^2 was covered by the CIGS. Assuming a 10% efficient cell, the power output of array was expected to be 18.3 W under AM1.5 conditions. For all measurements of the solar array, the Amprobe SOLAR-600 Solar Power Analyzer was used. This solar analyzer produced IV curves for all measurements and also displayed maximum power point data. Through repeated testing on a relatively cloudy day in Monterey, CA, where the average solar irradiance is less than AM1.5, the average power generated by the array was 11.2 W. At this maximum power point, the voltage was approximately 14.0 V and the current was roughly 800.0 mA. It was found that any losses from the modular design were negligible and that the power cable connections performed as intended. A typical IV curve of the final array is presented in Figure 32. The fill factor averaged a disappointing 56.9% on the first day of testing; however, the power generated by the array was promising.

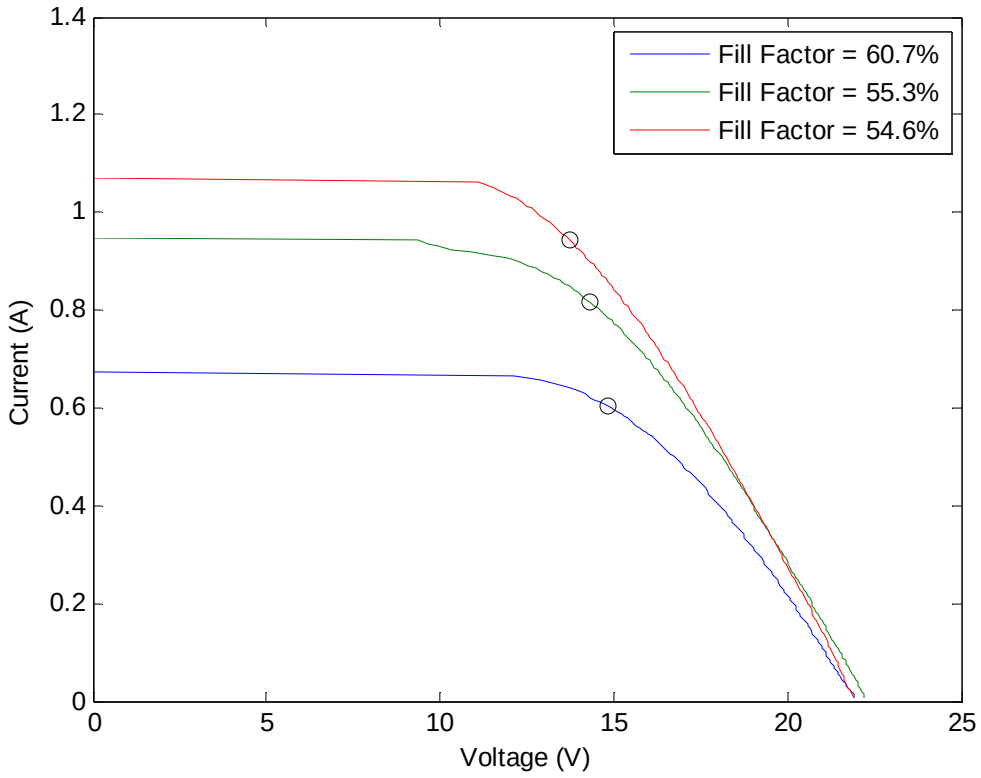

Figure 32. IV curves for the final solar array with the maximum power point indicated.

2. MPPT, Boost Controller, and Balance Charger Incorporation

Since the fill factor and IV characteristics of the array were less than optimal, it was imperative to have an effective MPPT and Boost Controller. The MPPT chosen for this research was a combined MPPT and Boost Controller that was also utilized in [8]. The SPV1020 DC-DC boost converter by ST Microelectronics utilizes an embedded MPPT algorithm that advertises an efficiency of up to 98%. This MPPT/Boost Controller was chosen because of its high efficiency and low weight. In [8], the SPV1020 failed to achieve the levels of efficiency desired; in that research the input voltage was partitioned to 6.0 V with respect to the intended output voltage of 24.2 V. Boosting the voltage by a factor of four greatly reduced the efficiency of the DC-DC converter. This research focused on increasing the voltage of the array to reduce the stress on the DC-DC converter and increase the overall efficiency of the system. To accommodate the modular array's measured open circuit voltage of 22.0 V, it was necessary to replace a

chip resistor on the SPV 1020. By replacing the R_2 resistor on the circuit board, the output voltage of the device remained at 24.2 V, but the input voltage was scaled to 20.5 V according to the equation in [40],

$$\frac{R_1}{R_2} = \frac{V_{OC}}{1.25} - 1 \ . \tag{6}$$

The resistor values for the MPPT/Boost Controller are shown in Table 7. Specifications and schematics for the SPV 1020 can be found in [40].

Table 7. The resistance of the surface mounted resistors used for voltage partitioning in the MPPT/boost controller.

Parameter	Value (ohms)
R_1	732 k
R_2	47 k
R_3	2.55 M
R_4	110 k

To verify the MPPT was operating effectively, a 50.0 Ω, high power resistor was used to simulate the Raven B, DDL as shown in Figure 33. By measuring the current and voltage at each node in the circuit, it was shown that the MPPT/Boost Controller maintained an output voltage of 24.0 V while the array operated at its maximum power point, corresponding to a voltage of 14.0 V. Proving the MPPT accurately tracked the voltage and the DC-DC converter appropriately boosted the voltage, we determined the SPV1020 was properly configured for the integration with the Raven system.

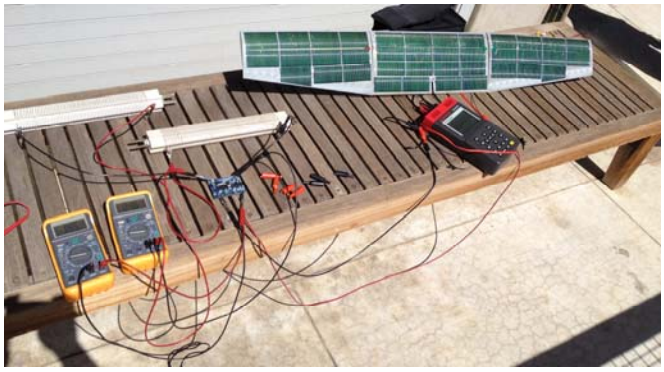

Figure 33. A load test of the MPPT/boost controller to confirm the functionality of the power circuit equipment.

Finally, a balance charger was required as discussed in Chapter IV. The balance charger chosen was the Ultra-Balancer from Common Sense RC. The proven track record of the balance charger in [6] and [8] combined with its sleek design and light weight made it an easy choice.

3. System Configuration

The final configuration of the system components is shown in Figure 34. The solar array is connected to the SPV1020 MPPT/Boost Controller followed by the Li-ion battery with the balance charger in parallel. A blocking diode to stop current flow from the battery to the solar array was unnecessary because it is incorporated in the SPV1020 schematic [39]. Finally, the Raven AV is linked to the battery. With the power circuitry assembled, full system testing was possible. During testing, the current and voltage supplied to the AV was monitored using LabVIEW, while the power supplied by the array was measured with handheld multimeters. A fan was positioned next to the solar array in order to reduce temperature effects on the array and simulate the cooling effect caused by the passage of wind over the wing.

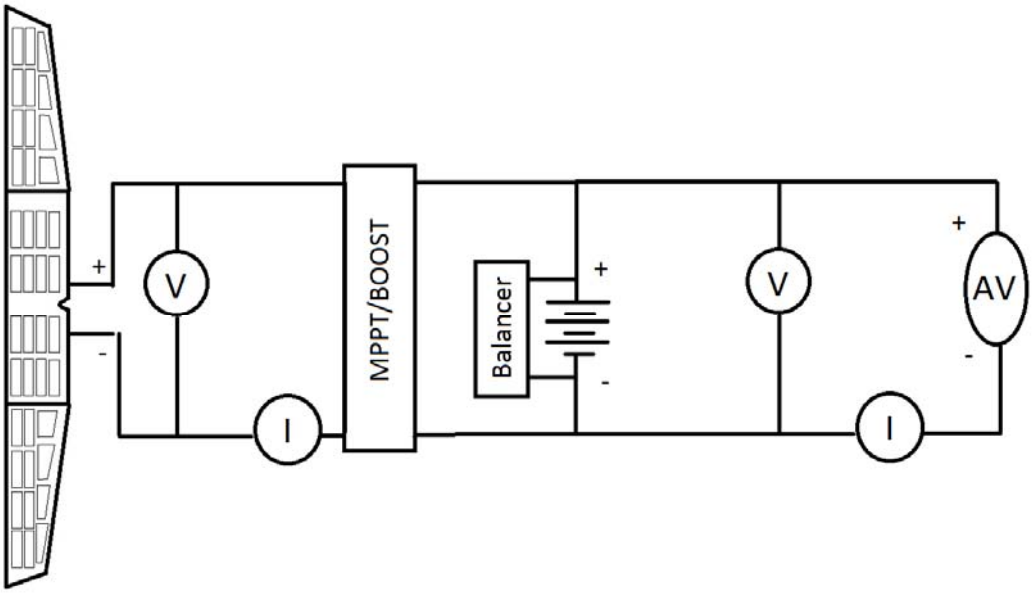

Figure 34. The test configuration for the solar-powered Raven B, DDL.

D. FULL SYSTEM TESTING

1. Results of Integrated System

Prior to full system testing, the solar array was inadvertently subjected to a water intrusion test. Recent rains in Monterey Bay caused the roof of the solar lab to leak, and the solar array sat in a small layer of water for up to 48 hours. Upon cleaning and drying the wing, the output of the CIGS remained unchanged compared to baseline tests. Therefore, results of the water intrusion test support the hypothesis that with proper encapsulation a solar integrated wing is appropriately protected from the elements.

Once it was determined the solar array was undamaged from the water intrusion test, full system testing commenced. The integrated system was evaluated in the same fashion as the baseline endurance tests. The test started when the battery was connected to the AV and concluded when the GCS indicated a low voltage warning of 21.9 V. As conducted previously, the throttle was set to 100% for the first 20 s before it was reduced to 50% throttle for the remainder of the trial. The tests were conducted on the roof of Spanagel Hall at the Naval Postgraduate School in Monterey, California, and each trial was conducted between the hours of 1100 and 1600. Cloud cover was minimal throughout testing; however, periodic clouds would shade the array and cause the power output to fluctuate. A picture of the actual test set up is shown in Figure 35.

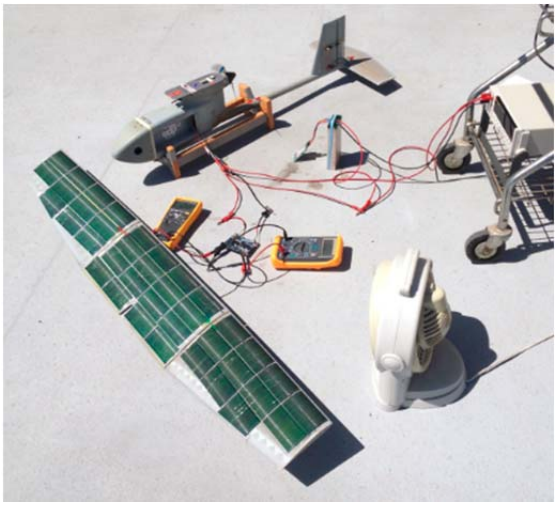

Figure 35. The test set-up for the full system configuration

In total, six different batteries and two fuselages were used for six trials of the solar tests. At the conclusion of testing, it was determined that the endurance of the AV with the solar array attached increased by an average of roughly 15 minutes, corresponding to an increase of 48.87%. A graph of the solar tests compared with the baseline is presented in Figure 36. It is immediately apparent from Figure 36 that the magnitude of the general slope of the solar tests is less than that of the baseline. This slope was expected because the power provided by the array would reduce the discharge rate of the battery voltage. The measured endurances from the solar tests covered a greater range than the baseline; however, this was due to the fluctuations in solar irradiance and atmospheric conditions at the time of testing.

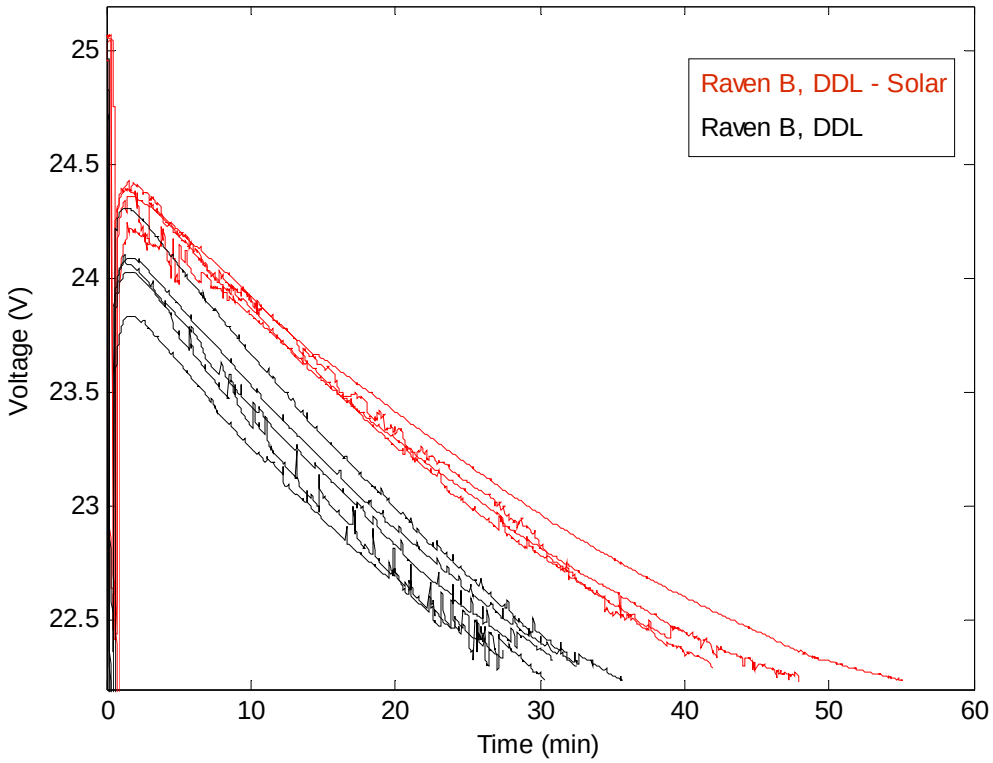

Figure 36. The results of a solar integrated Raven B, DDL endurance test compared to the baseline endurance.

A summary of the solar integrated tests is listed in Table 8. Of note, the average power shown in Table 8 is significantly lower than the values from the baseline tests in Table 6. Calculating the difference in power supplied from the battery during each phase of testing gives the power generated by the solar array. Averaging 14.9 W, this magnitude is consistent with the observed output of the MPPT. To confirm this observation, the IV characteristics of the array were investigated. Before each trial, the IV characteristics of the array were measured with the solar analyzer to produce the IV curves illustrated in Figure 37. From Figure 37, it is seen that the solar analyzer measured the maximum operating point at an average of 14.1 W. During testing, the MPPT fixed the array's operating point near the maximum power points indicated by the circles in Figure 37. Depending upon the irradiance during each subsequent trial, the operating point would fluctuate to provide the maximum power to the MPPT which was then boosted to 24.2 V and delivered to the AV at approximately 0.56 A. Therefore, the predicted output power of the array closely matches the data collected during endurance testing.

Table 8. The results of the solar integrated Raven B, DDL endurance tests.

Test	Time (min)	Percent Increase (%)	Average Power from Battery (W)
1	38	26.79%	63.89
2	47.97	60.06%	54.39
3	44.71	49.18%	53.48
4	39.92	33.20%	53.85
5	41.98	40.07%	54.34
6	55.12	83.92%	53.19
Averages	**44.62**	**48.87%**	**55.52**

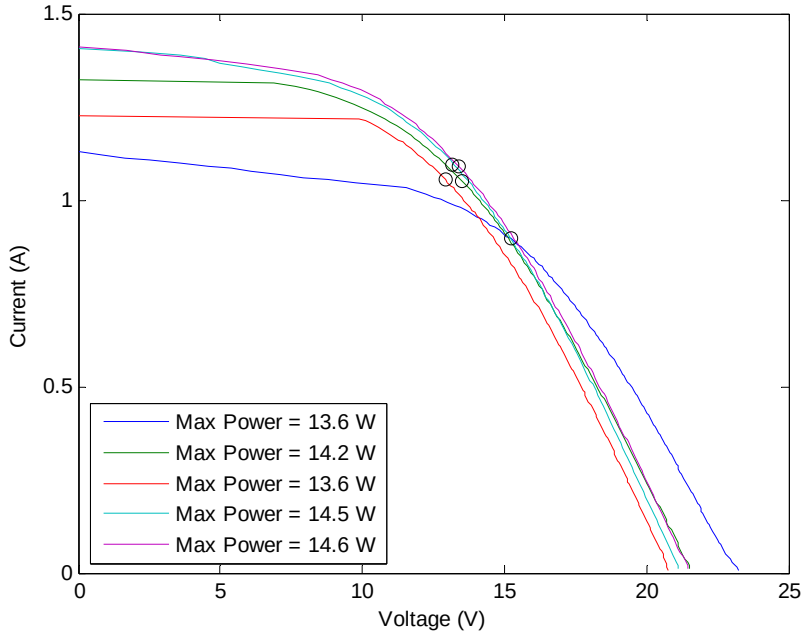

Figure 37. The IV characteristics of the solar array measured prior to endurance testing.

As discussed previously, the power requirement of the current IR and EO payloads is approximately 6.0 W. The measured 14.0 W provided by the array is more than sufficient to handle the power requirements of the payloads. Furthermore, the array has an additional 8.0 W available to extend the endurance of the AV, power simultaneous payloads, or handle a single, more demanding payload. In summation, the solar array would provide flexibility to the Raven B, DDL platform.

2. Full System Testing with Greater Efficiency CIGS

For the low-efficiency CIGS used in this research, 14.9 W were provided to the AV. More efficient cells will increase that power production because they will provide a higher level of short-circuit current for the same open-circuit voltage. As an example, if the efficiency of the cells were doubled under AM1.5 conditions, the array would be expected to double the output power of what was witnessed in this research. With an output power of 30.0 W, these CIGS would extend the endurance of the AV to approximately 2.0 hours, according to

$$\frac{\left[\left(\frac{98W\cdot hour}{25.2V}\right)-\left(\frac{20\,\mathrm{s}}{(60)(60)}\right)(18.25A-1.12A)-\left(\frac{15\,\mathrm{min}}{60}\right)(2.79A-1.12A)\right]}{(2.79A-1.12A)}=2.0\,\mathrm{hrs.} \quad (7)$$

In (7) the battery capacity of 98 W-hours is reduced by the energy required to maintain a throttle position of 100% for 20 s and an AV retrograde of 15 minutes. The adjusted battery capacity is then divided by the current drawn from the battery at the 50% throttle setting. Additionally, all currents from Table 5 and listed in (7) are reduced by the amount of current provided by the array. This solution fails to account for a safety factor so that the Li-ion batteries do not discharge to dangerous levels; however, it is an appropriate approximation.

3. Cost of Implementation

It is possible that using more efficient TFPV cells may be a cost-prohibitive endeavor with respect to the cost of the Raven system. For fiscal year 2013, the Raven system cost $110,000, or approximately $36,000 per AV according to [41]. The CIGS utilized in this research cost $100, and the associated power circuitry accounted for an additional $150 [6],[8]. Including labor and miscellaneous equipment, it is estimated that the cost required to outfit the Raven system would be roughly $1000 [6]. However, it is assumed that the price per unit would drop if implemented across the entire fleet. For the relatively low power requirements of the analog variant, the increase in price for the Raven system is sensible as discussed in previous theses. Conversely, for the digital Raven B, DDL, the user receives fewer benefits at the same cost. As TFPV technology matures and the price per watt reduces further to an economical level with respect to the cost of the platform, the concept appears to be an effective way to boost power production at a relatively low cost [41].

E. SCAN EAGLE APPLICATION

Since the current draw of the Raven has increased between the variants, the feasibility of developing a solar powered UAV from the current DOD inventory appears less likely than previous research indicated. However, as stated, the ability of a TFPV array to power additional payloads is a promising alternative. Not only can this concept

be applied to Group 1 UAVs, the integration of TFPVs with Group 2 and Group 3 assets can expand the payload capacity of the existing platforms. While the endurance of these larger, gas-powered UAVs is quite substantial, the payload capacity is limited. Solar integration expands that capacity for day time operations at a relatively low cost. For example, the approximate useable surface area of a Scan Eagle is 5900 cm^2 when only the wings are utilized for TFPV application. This sized array would generate a substantial amount of power for additional payloads with minimal weight added to the AV. A comparison of the power generation of a solar integrated Scan Eagle under various AM conditions and TFPV efficiencies is calculated in Table 9 from (5).

Table 9. Comparison of power generated by a TFPV integrated Scan Eagle at varying efficiencies and air mass.

Air Mass	Efficiency of TFPV	Power Generated
1000 W/m2	10%	59.0 W
	15%	88.5W
750 W/m2	10%	44.3 W
	15%	66.4 W
500 W/m2	10%	29.5 W
	15%	44.3 W

It is expected that with the power provided by the array in Table 9, the Scan Eagle is capable of powering additional payloads without taxing the engine or consuming any of the battery life during daytime operations.

THIS PAGE INTENTIONALLY LEFT BLANK

VI. CONCLUSIONS AND RECOMMENDATIONS

The methods and limitations of expanding the payload capacity and extending the endurance of the RQ-11B, DDL Raven system by outfitting the wing with an array of CIGS solar cells were explored in this thesis. To start, this research examined current DOD policy regarding renewable energy sources and fiscal constraints of the current economy in Chapter I. Then, in Chapter II, the UAV inventory was introduced, and the RQ-11 Raven system and its multiple variants were explored. Capitalizing on the efforts of previous research at the Naval Postgraduate School and to provide a point of comparison, we focused primarily on the Raven system.

Once the subject platform was adequately described, the basics of the photovoltaic effect and various types of TFPVs were discussed in Chapter III. Due to their listed advantages and current availability, CIGS were chosen for integration. In order to demonstrate how the CIGS could be evaluated and incorporated with the Raven system, the associated power circuitry was introduced and selected in Chapter IV. With the background information and design solidified, experimentation began by establishing a baseline of performance in Chapter V. This baseline was then used to evaluate the benefits of the fully integrated design.

A. ANALYSIS OF FINDINGS

The design of the CIGS array in this research focused on creating a product that maintained the expeditionary and modular nature of the current platform. Choosing to utilize traditional power cables in place of the wing pin and cup connectors that are currently utilized in the Raven, we found that an array could be incorporated in the wing with undetectable power losses as a result of the additional connections. Over the course of the testing process, one of the connectors loosened from use. It became loose because it was not sealed in place with the procedures listed in the maintenance manual for replacement of the pin and cup due to asset availability. If sealed and aligned properly, the power cable would have fared better during testing. If implemented in the fleet, it is recommended that a more robust power cable be designed specifically for the wing. This

cable should maintain the structural integrity of the current system but utilize the concept set forth in this research. One idea would be to use a smaller power cable that may be housed in the existing pin and cup.

An important contribution of this thesis occurred during establishment of a performance baseline and the validation of the previous research conducted in [6] and [8]. Monitoring the current and voltage during ground tests, it was immediately apparent that the Raven B, DDL variant had much higher power requirements than previous variants. After multiple iterations of testing and research, it was confirmed that the Raven B, DDL consumed two to three times the current as the analog versions of the platform. At this point in the research, the endurance enhancements predicted by the CIGS array designed in [6] and [8] were no longer valid. Further testing was required to determine the actual endurance of the platform and the increase in endurance established by an incorporated solar array.

Averaging a baseline endurance of only 30 minutes before reaching the low battery voltage warning, the CIGS array enabled the AV to operate for nearly 45 minutes under similar test conditions. With a solar array integrated with the AV, a 48.87% improvement was documented over the course of six trials. It is expected that in environments with greater solar irradiance and more efficient cells that this figure will improve; however, geography cannot dictate the employment of this platform. The improvements made to the Raven B, DDL variant drastically diminished the endurance benefits of incorporating a TFPV array with the power circuitry.

While the endurance benefits were hampered by the improvements to the digital Raven platform, the power produced by the array may still be harnessed and applied elsewhere in the system. Payload testing concluded that approximately 6.0 W are required to operate a single payload. The 14.0 W generated by low efficiency CIGS are more than sufficient to expand the payload capacity of the Raven. With higher efficiency TFPVs, that benefit increases tremendously.

Ultimately, with the current efficiencies of TFPVs and the increased power requirements of the Raven RQ-11B, DDL variant in mind, the concept of a completely

solar powered Raven is less likely. However, the benefits of a TFPV array integrated with the wing are not limited to endurance. An expansion of the payload capacity would benefit the warfighter by expanding the capabilities and the potential mission set of the platform. Additionally, the solar wing would provide a much needed power source in austere and isolated environments.

B. RECOMMENDATIONS FOR FUTURE WORK

1. Verify Current Consumption of Raven RQ-11B, DDL

The power consumption of the RQ-11B, DDL in this research was almost triple the consumption of the analog RQ-11B. To confirm these findings, a broad range of RQ-11B, DDL systems should be tested to confirm that the high power requirements are not an anomaly for the Raven system that was provided by PMA-263.

2. Measure the Current of AV in Autonomous Flight

When placed in autonomous mode, the user has no indication of the throttle position or power drawn from the battery. It is possible that in autonomous mode, the motor's speed controller throttles down to a lower current draw in order to maintain a 26 knot cruising speed. Until the current and voltage are measured in flight, the true power consumption of the Raven may differ from the ground tests in this research.

To conduct these measurements, a simple data logger could be incorporated in the AV circuitry to periodically sample the voltage and current provided by the battery. This information will also be useful for endurance simulations from past research.

3. Conduct Research with Gas Powered Motors

Simplistic calculations to determine the potential power generation of an array installed on the Scan Eagle were provided in this research; however, the concept can be applied to a wide range of Group 2 and Group 3 UAVs. These UAVs provide a much larger surface for solar integration and would reduce the horsepower requirements of the motor by powering the payloads during daytime operations. This power balancing can extend both the capabilities and endurance of larger platforms.

4. Refine the Wing Interface Design

Since the power cables that replaced the wing pin and cup were of a rudimentary design, further research is required to create a connector that provides the structural integrity and reliability provided by the existing interface. This research is required before the concept could be implemented.

APPENDIX. PROCEDURES TO REPLACE WING CONNECTORS

A. WING PIN REPLACEMENT PROCEDURES

1	Heat the wing pin with a solder tip or torch until the epoxy becomes tacky.
2	Remove pin with pliers and let cool.
3	Smooth out vacancy with drill bit to increase size of hole to 0.9cm wide and 4cm deep.
4	Drill small hole into underside of wing, 4cm from connection side of wing
5	Place male end of power cable assembly P/N 839-1173-N, MFG P/N 10-00464 in vacancy.
6	Feed cable leads through small hole in underside of wing.
7	Apply epoxy or sealant to power cable and vacancy.
8	Maintain proper alignment of cable assembly and let cure.

B. WING CUP REPLACEMENT PROCEDURES

1	Insert a drill bit that fits snug in wing cup. Heat drill bit with a solder tip or torch until it expands and the epoxy becomes tacky.
2	Remove bit and wing cup with pliers and let cool.
3	Smooth out vacancy with drill to increase hole to 0.9cm wide and 5.5cm deep.
4	Drill small hole into underside of wing, 5.5cm from connection side of wing
5	Place female end of power cable assembly P/N 839-1173-N, MFG P/N 10-00464 in vacancy.
6	Feed cable leads through small hole in underside of wing.
7	Apply epoxy or sealant to power cable and vacancy.
8	Maintain proper alignment of cable assembly and let cure.

THIS PAGE INTENTIONALLY LEFT BLANK

LIST OF REFERENCES

[1] Department of Defense. "Unmanned systems integrated roadmap FY2013–2038," DOD, Washington, DC, Reference Number 14-S-0553., 2013 [Online]. Available: http://www.defense.gov/pubs/DOD-USRM-2013.pdf

[2] United States Marine Corps, "2012 U.S. Marine Corps S&T strategic plan: leading edge technology for Marines of tomorrow," DOD, Washington, DC, 2012 [Online]. Available: http://www.hqmc.marines.mil/Portals/160/Docs/USMC%20S_T%20Strat_Plan_2012_Final_31_%20Jan.pdf

[3] North Central Texas Council of Governments, "North Central Texas regional general aviation and heliport system plan," North Central Texas Council, Arlington, Texas, 2011 [Online]. Available: http://www.nctcog.org/aa/jobs/trans/aviation/plan/UnmannedAircraftSystemsReport.pdf

[4] D. Kuhn. (2009, Oct. 19). Unmanned Aerial Vehicles keep watch in Afghanistan. *American Forces Press Service* [Online]. Available: http://www.defense.gov/News/NewsArticle.aspx?ID=56281

[5] Northrop Grumman. (2014, Jan.). *Global Hawk* [Online]. Available: http://www.northropgrumman.com/capabilities/globalhawk/Pages/default.aspx

[6] J. V. Coba, "Application of copper indium gallium diselenide photovoltaic cells to extend the endurance and capabilities of the Raven RQ-11B Unmanned Aerial Vehicle," M.S. thesis, Dept. of ECE, Naval Postgraduate School, Monterey, California, 2009.

[7] W. Hurd, "Application of copper indium gallium diselenide photovoltaic cells to extend the endurance and capabilities of unmanned aerial vehicles," M.S. thesis, Dept. of ECE, Naval Postgraduate School, Monterey, CA, 2009.

[8] C. Gromadski, "Extending the endurance of small unmanned aerial vehicles using advanced flexible solar cells," M.S. thesis, Dept. of ECE, Naval Postgraduate School, Monterey, CA, 2012.

[9] MicroLink Devices. (2013). *Photovoltaics* [Online]. Available: http://mldevices.com/index.php/products-a-services/photovoltaics

[10] AeroVironment. (2014). *UAS: RQ-11B Raven* [Online]. Available: http://www.avinc.com/uas/small_uas/raven/

[11] *Raven B Small Unmanned Aircraft System with Digital Data Link Operator's Manual,* Rev. B., DOD, Washington, DC, Reference Number 60707_A1., 2012.

[12] Defense Industry Daily Staff. (2012, Apr. 12). Ravens, mini-UAVs winning gold in Afghanistan's commando 'Olympics'. *Defense Industry Daily* [Online]. Available: http://www.defenseindustrydaily.com/raven-uavs-winning-gold-in-afghanistans-commando-olympics-01432/

[13] D. Wasserbly. (2009 Aug. 18). US Army's Raven datalinks to go digital. *International Defense Review* [Online]. Available: IHS Jane's, https://janes.ihs.com/CustomPages/Janes/DisplayPage.aspx?DocType=News&ItemId=+++1106519&Pubabbrev=IDR [Accessed March 12, 2014]

[14] IHS Jane's. (2013, Aug. 19). *AeroVironment Raven* [Online]. Available: http://search.janes.com. [Accessed March 12, 2014]

[15] AeroVironment. (2014). *UAS: WASP AE* [Online]. Available: http://www.avinc.com/uas/small_uas/waspAE/

[16] AeroVironment. (2014). *UAS: RQ-20A Puma AE* [Online]. Available: http://www.avinc.com/uas/small_uas/puma/

[17] K. Johnson. (2008 Jan. 22). Downside of full combat load examined. *Marine Corps Times* [Online]. Available: http://www.marinecorpstimes.com/article/20080122/NEWS/801220310/Downside-of-full-combat-load-examined

[18] Draganfly Innovations Inc. (2014). *DraganFly Tango* [Online]. Available: http://www.draganfly.com/uav-airplane/tango/

[19] Dara Aviation Inc. (2006). *Dara Aviation specializing in the innovation and development of lightweight Unmanned Aerial Vehicles* [Online]. Available: http://www.daraaviation.com/index.html

[20] National Renewable Energy Laboratory. (2014 Mar. 19). *Silicon materials and devices R&D* [Online]. Available: http://www.nrel.gov/ncpv/images/efficiency_chart.jpg

[21] MiaSolé. (2011 Oct.). *MS Series -03 PV Module* [Online]. Available: http://www.miasole.com/node/170

[22] Green Rhino Energy Ltd. (2013). *Defining standard spectra for solar panels* [Online] Available: http://www.greenrhinoenergy.com/solar/radiation/spectra.php

[23] C. Honsberg and S. Bowden. (2014). *PVCDROM* [Online]. Available: http://www.pveducation.org/pvcdrom/

[24] R. A. Rohde. (2007 Jun. 09). *Solar radiation spectrum* [Online]. Available: http://www.globalwarmingart.com/wiki/File:Solar_Spectrum_png

[25] A. S. Grove, "Elements of semiconductor physics," in Physics and Technology of Semiconductor Devices, Palo Alto: John Wiley and Sons Inc., 1967, ch. 4, sec. 4.1, pp. 91-95.

[26] Sherif Michael, "EC3240 renewable energy at military bases and for the warfighter, 2013," unpublished.

[27] National Renewable Energy Laboratory. (2012 Apr. 25). *Silicon materials and devices R&D* [Online]. Available: http://www.nrel.gov/pv/silicon_materials_devices.html

[28] U.S. Department of Energy. (2013 Oct.). *Photovoltaics research and development* [Online]. Available: http://energy.gov/eere/sunshot/photovoltaics-research-and-development

[29] A. Kanevce, "Anticipated performance of Cu(In,Ga)Se2 solar cells in the thin-film limit," Ph.D. dissertation, Dept. of Physics, Colorado State Univ., Fort Collins, 2007.

[30] National Renewable Energy Laboratory. (2011 Oct. 06). *Polycrystalline thin-film materials and devices R&D* [Online]. Available: http://www.nrel.gov/pv/thinfilm.html

[31] C. Stevenson, "Utilizing maximum power point trackers in parallel to maximize the output of a solar (photovoltaic) array," M.S. thesis, Dept. of ECE, Naval Post Graduate School, Monterey, CA, 2012.

[32] *Solar Cell Array Design Handbook,* Vol.1., NASA Jet Propulsion Lab., Pasadena, CA, 1976, pp. 3.5-1.

[33] D. Ragonese and M. Ragusa. (2012, May). AN3392 application note – designing with the SPV 1020, and interleaved boost converter with MPPT algorithm. STMicroelectronics, Geneva, Switzerland. [Online]. Available: http://www.st.com/st-webui/static/active/en/resource/technical/document/application_note/DM00026751.pdf

[34] R. A. Cullen, (2009). *What is maximum power point tracking (MPPT) and how does it work?* [Online]. Available: http://www.blueskyenergyinc.com/uploads/pdf/BSE_What_is_MPPT.pdf

[35] N. Mohan, T. Undeland and W. Robbins,"DC-DC switch mode converters," in *Power Electronics: Converters, Applications, and Design.* 3rd ed. New Delhi, India: Wiley India, 2006, ch. 7, sec. 4, pp. 161-183.

[36] K. Adkins, private communication, Feb 2014.

[37] Department of the Army. “Army Unmanned Aircraft System Operations,” DOD, Washington, DC, Field Manual Interim No. 3-04.155., 2006 [Online]. Available: http://www.fas.org/irp/doddir/army/fmi3-04-155.pdf

[38] C. K. Chin, “Extending the endurance, missions, and capabilities of most UAVs using advanced flexible/ridged solar cells and new high power density batteries technology,” M.S. thesis, Dept. of ECE, Naval Postgraduate School, Monterey, CA, 2011.

[39] *Raven B Small Unmanned Aerial System Intermediate Level Repairs Manual,* DOD, Washington, DC, Reference Number 51582_D., 2008.

[40] Office of the Under Secretary of Defense (Comptroller)/ Chief Financial Officer, “Program acquisition cost by weapon system,” DOD, Washington, DC, 2014 [Online]. Available: http://comptroller.defense.gov/Portals/45/Documents/defbudget/fy2015/fy2015_Weapons.pdf

[41] V. Kapur, A. Bansal, and S. Roth, "Roadmap for manufacturing cost competitive CIGS modules," in *Photovoltaic Specialists Conference (PVSC), 38th IEEE*, 2012, pp. 1–2.

INITIAL DISTRIBUTION LIST

1. Defense Technical Information Center
   Ft. Belvoir, Virginia

2. Dudley Knox Library
   Naval Postgraduate School
   Monterey, California